Fatti non foste a viver come bruti,

ma per seguir virtute e canoscenza.

(Divina Commedia, Inferno, Canto XXVI, 119-120)

Preface

The aim of this Phd thesis is to get an insight on recent active seismic events occurring in the area of the Alps-Dinarides junction. This area is the most active on the northern rim of the Adria microplate due to the broader collision between the Eurasian plate and the African one.

Various studies have been performed on several recent events, from Joint Hypocentre Determination relocations, to source parameters waveform inversions, to understand the ongoing tectonic processes. A relevant part of the study has been taken also by the implementation of a synthetic seismogram software package based on the reflectivity method, useful to have waveform modelling at close epicentral distances, for seismic risk assessment.

Contents

List of Figures

List of Tables

Chapter 1

Alps-Dinarides Junction

1.1 Tectonic setting

The area under study is at the border between Italy, Slovenia and Austria. The main tectonic entities in the area are the Dinarides and Alpine arc, and the Adria microplate, a promontory, which could be part of the much bigger African plate [Channel and Horvath, 1976], [Platt et al., 1989], [Anderson and Jackson, 1987] and [Carulli et al., 1990].

The underlying mechanism for the seismicity in this area is the collision between the Eurasian plate and the Adria microplate. The relative movement of the two plates is around 5 mm per year, oriented 340 N [Aoudia, 1998]. In this area, and due to the approximately N-S oriented stress field [Bada et al., 2001], there are many recognized faults. Two main source mechanisms, each specific of a particular area can be distinguished. The Alpine area is mainly characterized by thrust mechanisms with fault

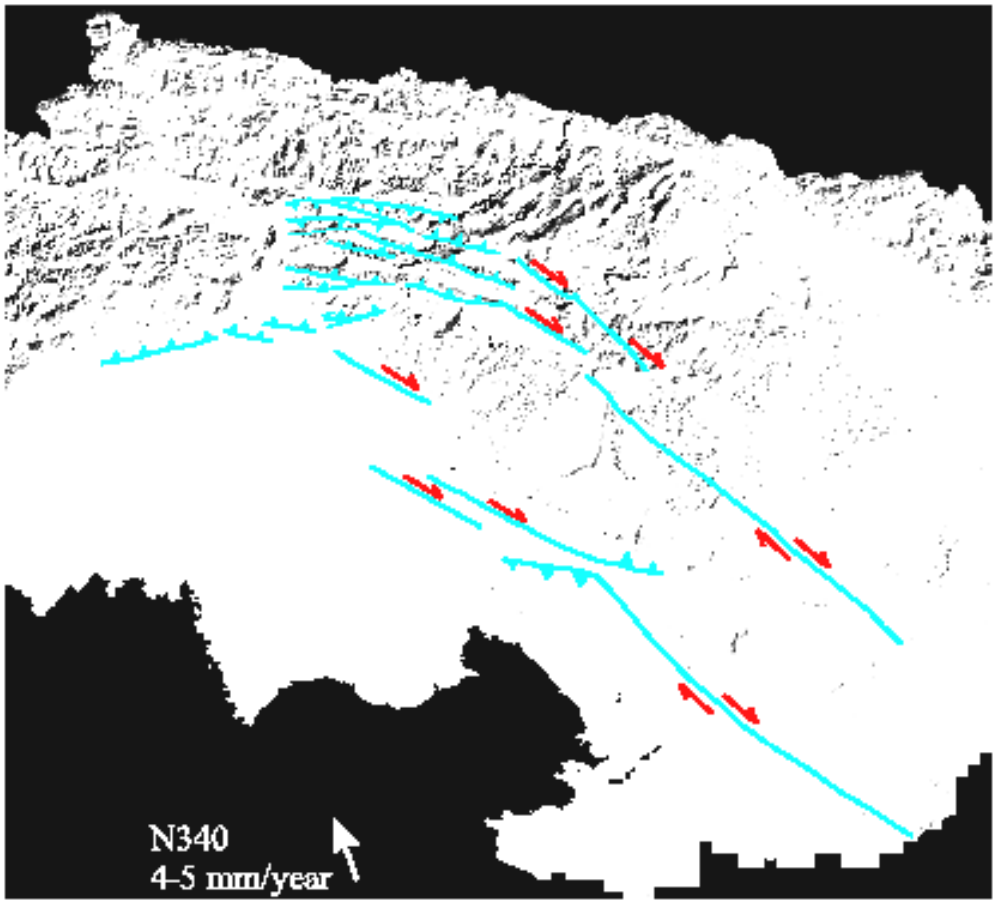

Figure 1.1: Active tectonic setting of the area [Aoudia, 1998]

planes in the $E-W$ direction, while the Dinaric area is mainly characterized by strike slip mechanisms, oriented $NW-SE$ [Poljak et al., 2000].

This region, however, is far from being simple. In detail we can identify from the tectonical point of view many smaller areas [Bressan et al., 2003], that make the transition between the two regimes softer. The two regimes, in fact, are a consequence of the same $N-S$ stress field acting on differently oriented structures.

1.2 Seismicity analysis

The strongest earthquake historically recorded in this area is the 1511 Idrija earthquake, a $M_S = 6.9$ event to the NE of Trieste [Fitzko et al., 2005], located on one of the main transform faults. In the last ten years the main activated seismogenetic areas have been the Bovec area, again transform faults and the nearby Friuli area, with thrust mechanisms.

Due to the tectonic setting, the area is extensively monitored with various networks, at least since the last ten years. The data available, both from Italian and Slovenian networks, is such that we can perform statistical analysis on the magnitudes of earthquakes occurred in the area.

The catalogue used is based on the Slovenian catalogue [Živčić et al., 2000] and on the $CRS-INOGS$ catalogue [INOGS, 2002]. The full catalogue used for this part of the study is plotted in Figure 1.2.

1.2.1 Gutenberg-Richter distribution

The most important relation in statistical studies on earthquake catalogues is the so called *Gutenberg Richter law*. N, the number of earthquakes for a given interval of magnitude, is function only of the average interval magnitude.

$$\log N = a + bM \tag{1.1}$$

The relation has been proven valid for different areas worldwide, which are characterized by the value of the two parameters a and b. In particular

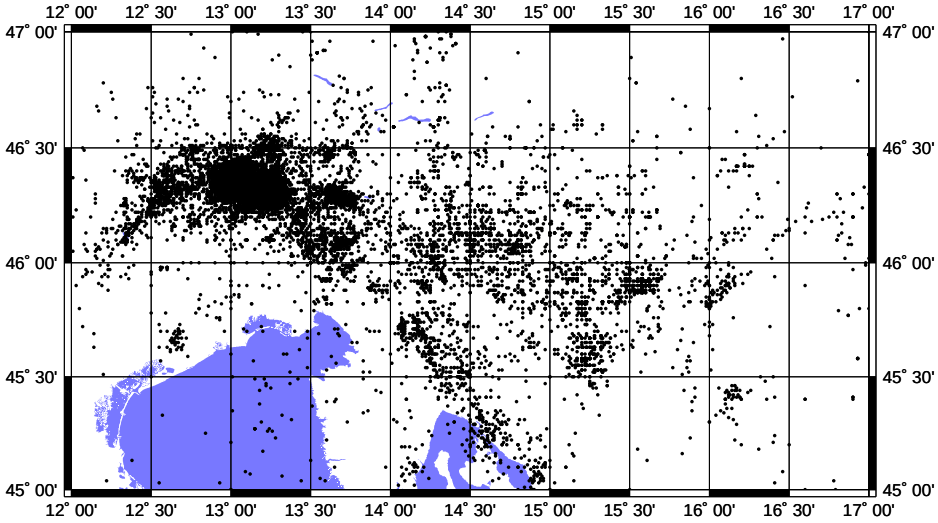

Figure 1.2: Full historical catalogue utilized for the study (1000-2002)

the value of b gives us some information on the tectonic stress characteristics of each area.

A simple relation [Utsu, 1965] can give us immediately the b estimate

$$b = \frac{0.4343}{M^* - M'} \tag{1.2}$$

where M^* is the average magnitude for events considered and M' is the minimum magnitude.

The *Gutenberg Richter law* implies the so called self similarity between earthquakes: it tells us that in every magnitude range the mutual relations between small and large earthquakes are the same.

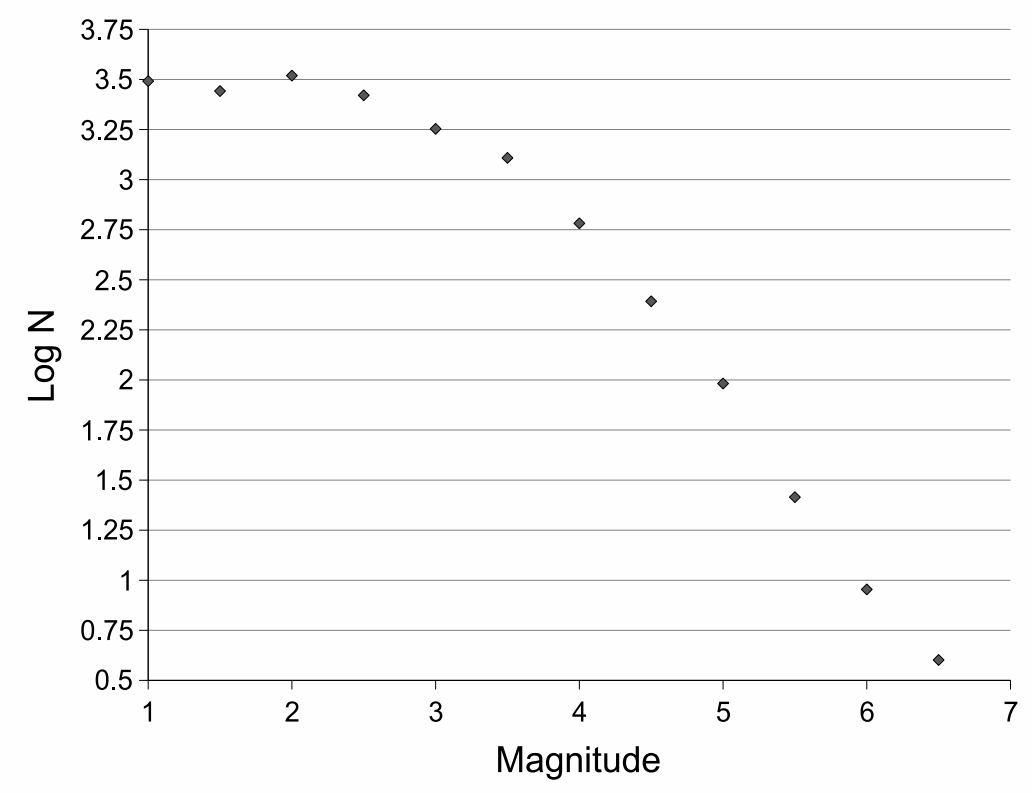

Figure 1.3: Completeness of the full catalogue of the area (1000-2002)

1.2.2 Catalogues and completeness

The most important parameter to be considered when working with a catalogue is the completeness threshold of the catalogue. This is the lowest value of magnitude for which we assume to have recorded, correctly located and hence estimated the magnitude of all earthquakes occurred in the time period of the catalogue in the studied area. When applying the Gutenberg Richter Law, we need to use data only for magnitude values above the completeness threshold.

Such analyses have been carried out on both the catalogues of Friuli and

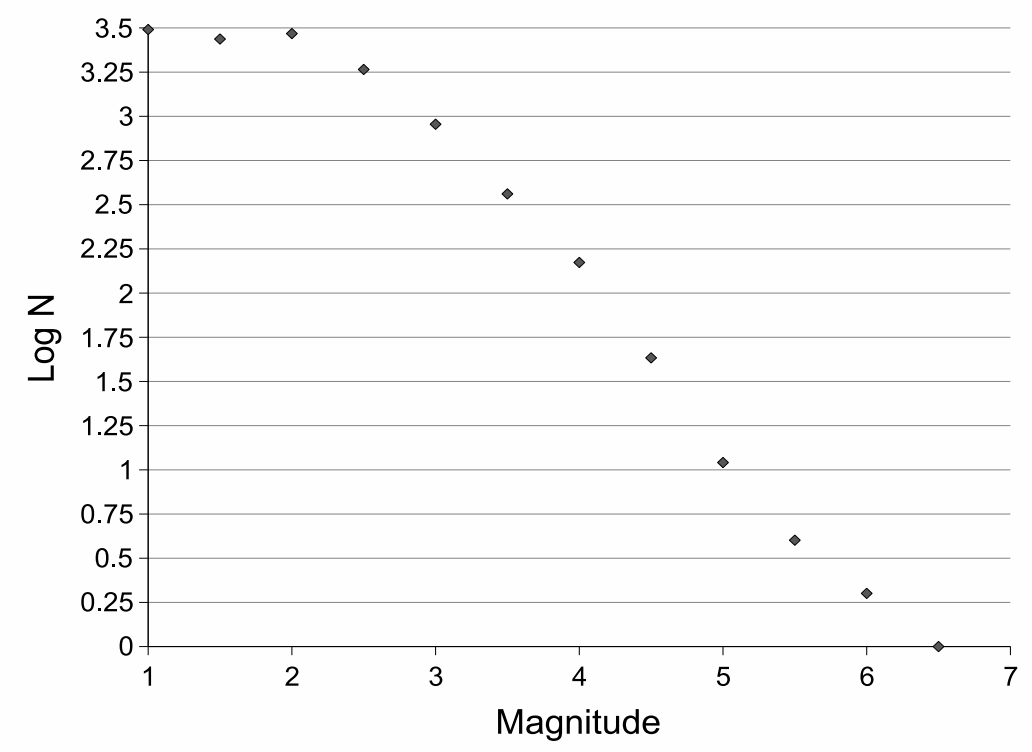

Figure 1.4: Completeness of the catalogue utilized for the study, for a smaller time interval (1976-2002)

Slovenia [Živčić et al., 2000]. Both have been considered complete up to a magnitude of 2.5 for the period 1976-2001 (see Figure 1.4).

1.2.3 Data analysis

In the framework of an undergraduate thesis at the Department of Earth Sciences of the University of Trieste [Viso, 2004] the question whether, apart from the differences in source mechanisms, the Dinaric (Slovenia) and the Alpine (Friuli) seismicity can be considered similar, has been studied.

The analysis of the two catalogues has been carried out with both the

least squares regression and the maximum likelihood method [Aki, 1965], obtaining similar results, maybe with a better fit for the maximum likelihood, which is also the most appropriate method to be used.

The b-value for the two catalogues has been estimated in 0.99, with a σ of 0.05. This value is compatible within the errors on the regressions with the values found for the two catalogues separately. The underlying tectonic source is the same, so we can suppose that, in spite of the differences in the slip mechanisms, the two areas have similar seismicity characteristics. We can therefore consider the whole area as homogeneous when considering its seismic behavior under stress.

Chapter 2

The Friuli Area

2.1 Overview

Friuli is sadly known to Italian people for the devastating earthquake that hit the area in 1976. This event has been therefore throughly studied in the last 20 years, see [Aoudia et al., 2000] and references therein.

2.1.1 Networks

In the area there are three complementary seismic networks operating: the *Rete Sismologica del Friuli-Venezia Giulia (RSFVG)* operated by the *Centro Ricerche sismologiche* of the *Istituto Nazionale di Oceanografia e Geofisica Sperimentale (CRS-INOGS)* using mainly short-period sensors for location purposes, the *Rete Accelerometrica del Friuli (RAF)* operated by the Department of Earth Sciences of the University of Trieste using accelerometers for shaking and site effects estimates, and the *North-East Italy Broad*

Date	Time	Lat. N	Long. E	M_D	Location
1977/09/16	23:48:06	46.370	13.016	5.2	TOLMEZZO
1978/04/03	10:49:46	46.304	13.139	4.2	GEMONA
1978/12/12	15:14:49	46.366	12.758	4.4	AMPEZZO
1979/04/18	15:19:18	46.379	13.276	4.8	CHIUSAFORTE
1983/02/10	22:30:34	46.269	13.395	4.2	UCCEA
1988/02/01	14:21:38	46.347	13.076	4.1	TOLMEZZO
1996/04/13	13:00:22	46.312	12.559	4.3	CLAUT
1998/05/28	09:32:19	46.295	13.049	4.1	TRASAGHIS
2002/02/14	03:18:02	46.426	13.100	4.9	M.SERNIO

Table 2.1: Events with $M_D > 4$ recorded by the OGS-CRS network

Band Network managed jointly by the two institutions.

2.1.2 Seismicity

After the strong event of 1976 there have been some moderate events distributed rather sparsely over all the area and located just below the Alpine piedmont area (Table 2.1).

For historical reasons, the *RSFVG*, which has the most complete catalogue for the area after the 1976 Friuli event, evaluates only the duration magnitude of events M_D.

2.2 Friuli 1976 scenario

2.2.1 Starting data

We take as a starting point the most recent study on the Friuli 1976 [Aoudia et al., 2000]. We adopt the proposed source model, concentrating on the near source ground motion, applying the reflectivity method. This is particularly important, since just above the fault area we can find many inhabited places (e. g. Gemona, Venzone) which have been almost completely destroyed during this earthquake.

The main event ($M_S = 6.5$) took place at 20:00 on May, 6 1976, located at $46.36N$ and $13.27E$. The finite grid of the extended source model is $18.5km$ along strike , $11km$ down deep with a total released seismic moment of $5.5 \cdot 10^{18} Nm$. The source mechanism has a strike of 288°, a dip of 29° and a rake of 112° The moment distribution [Aoudia et al., 2000] is plotted in Figure 2.2.

The modelling, carried out with a 1D structural model, neglecting the site effects, has been performed for a maximum frequency of $1Hz$. So we do not have to be surprised for the relatively low PGA found. We chose this upper frequency limit since we have a relatively simple source and structural model. The results are shown in Figure 2.3 where the peak acceleration has been computed on an evenly spaced grid covering the Friuli region. In Figure 2.4 we show an interpolated graph, related to Figure 2.3

Since the modelling has been carried out with a 1D structural model, all anomalies compared to a point source double couple radiation pattern are

due to the source finiteness and the rupturing modality. These are not very apparent and are restricted to the epicenter area just above and around the fault.

In fact in the area there are complex 3D structures, such as the alluvial fan of Gemona, for which a 1D model is not appropriate [Costa et al., 2006]. Future studies might deal with finite difference modelling of the fan area [Marrara et al., 2001] using the reflectivity method for the Green functions.

It is interesting to compare the scenario computed with the intensity obtained from macroseismic observation in Figure 2.5. While the shape of the radiation pattern is very similar, there is a significant difference in the orientation of the figure, that could lead us to suppose a strike angle towards 270° similar to that proposed in [Giorgetti, 1976]. This significant difference is probably due to the fact that the strike taken is coming from tectonical analysis, that consider the fault system not complanar, while we had to put them on the same plane. The faults are oriented as considered, but rather than complanar they are parallel and en-echelon.

2.3 Source Parameters inversion

For the Friuli 1976 event few near-source recordings are available. To get more insight on the modalities of the seismic energy release of the area we chose to study some recent events. Since about 10-15 years these have been recorded digitally, thus allowing us to apply modern waveform modelling techniques.

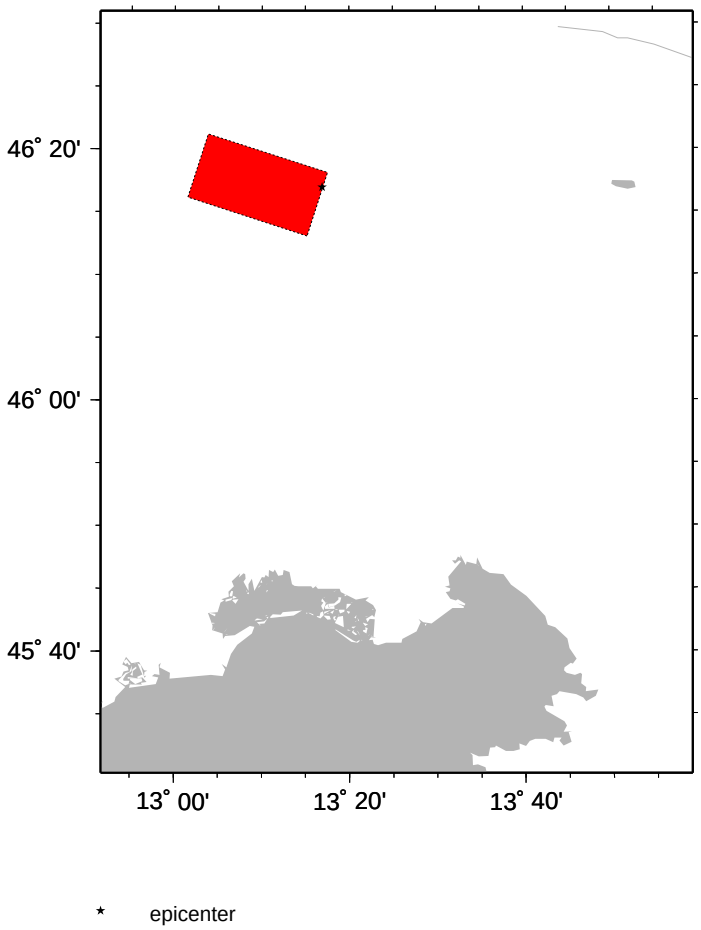

Figure 2.1: Fault used for the Friuli 1976 scenario

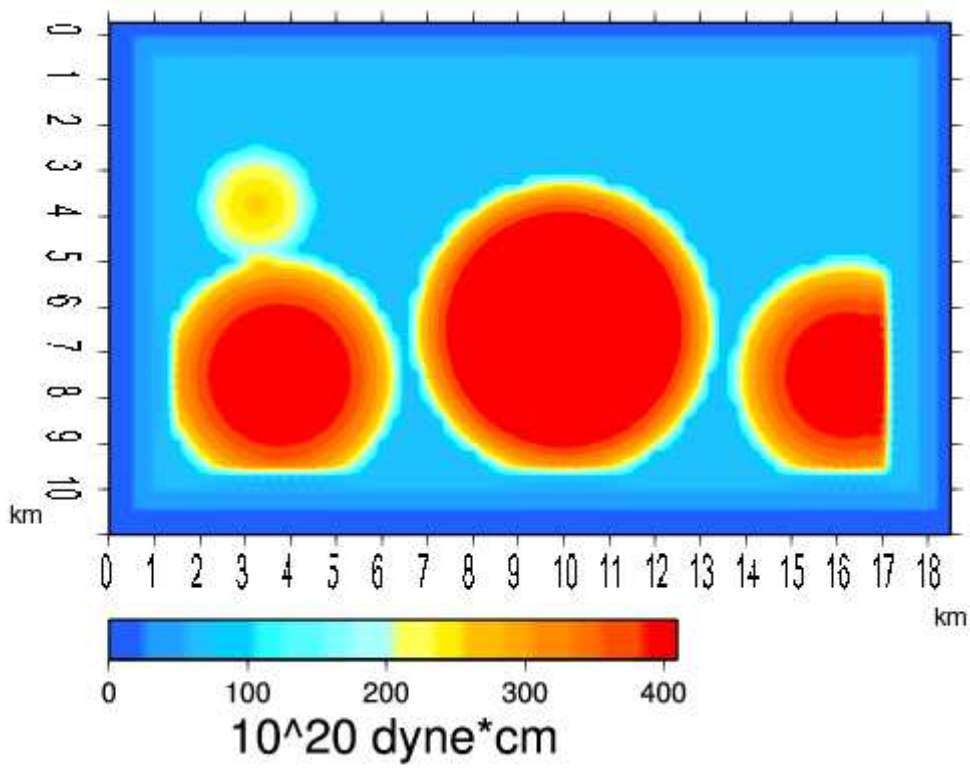

Figure 2.2: Moment distribution used to compute the 1976 scenario. Along strike lengths from East to West, depths from fault bottom upwards.

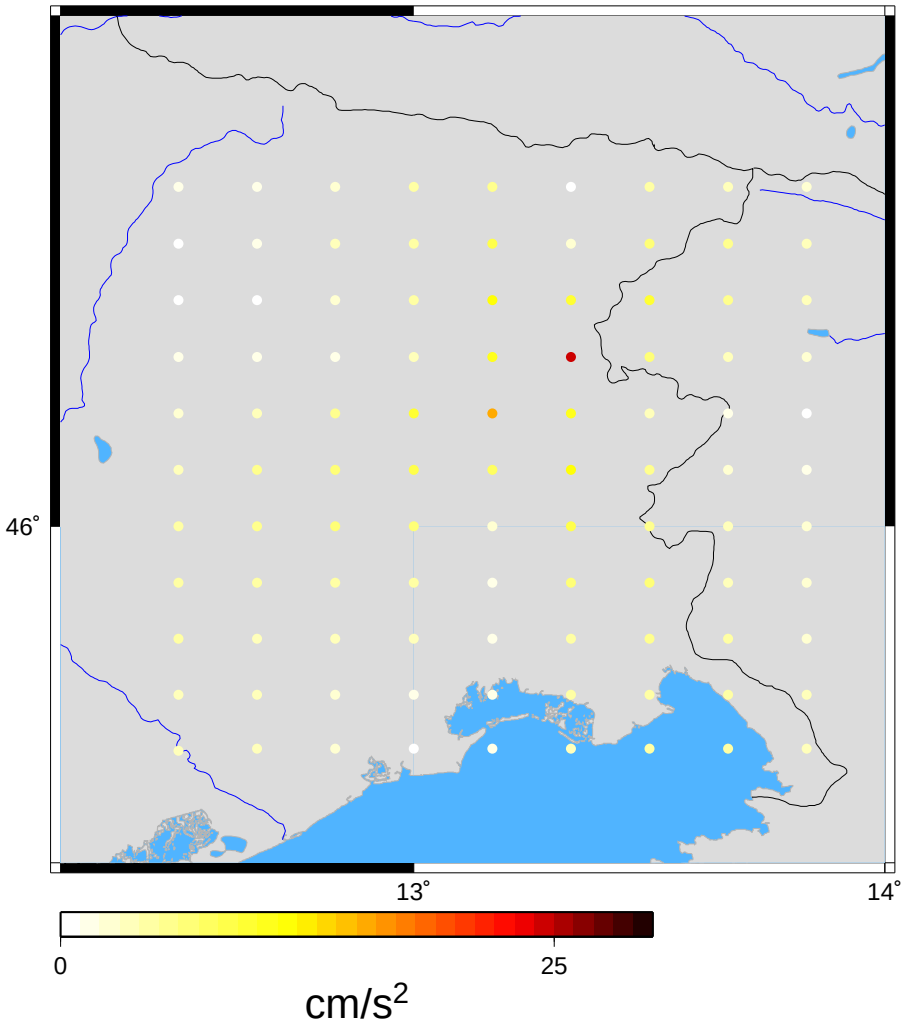

Figure 2.3: Computed peak accelerations (1 Hz maximum frequency)on an equally spaced grid from the source model of Figure 2.2 for the Friuli 1976 scenario. For the near source area see figure 2.6.

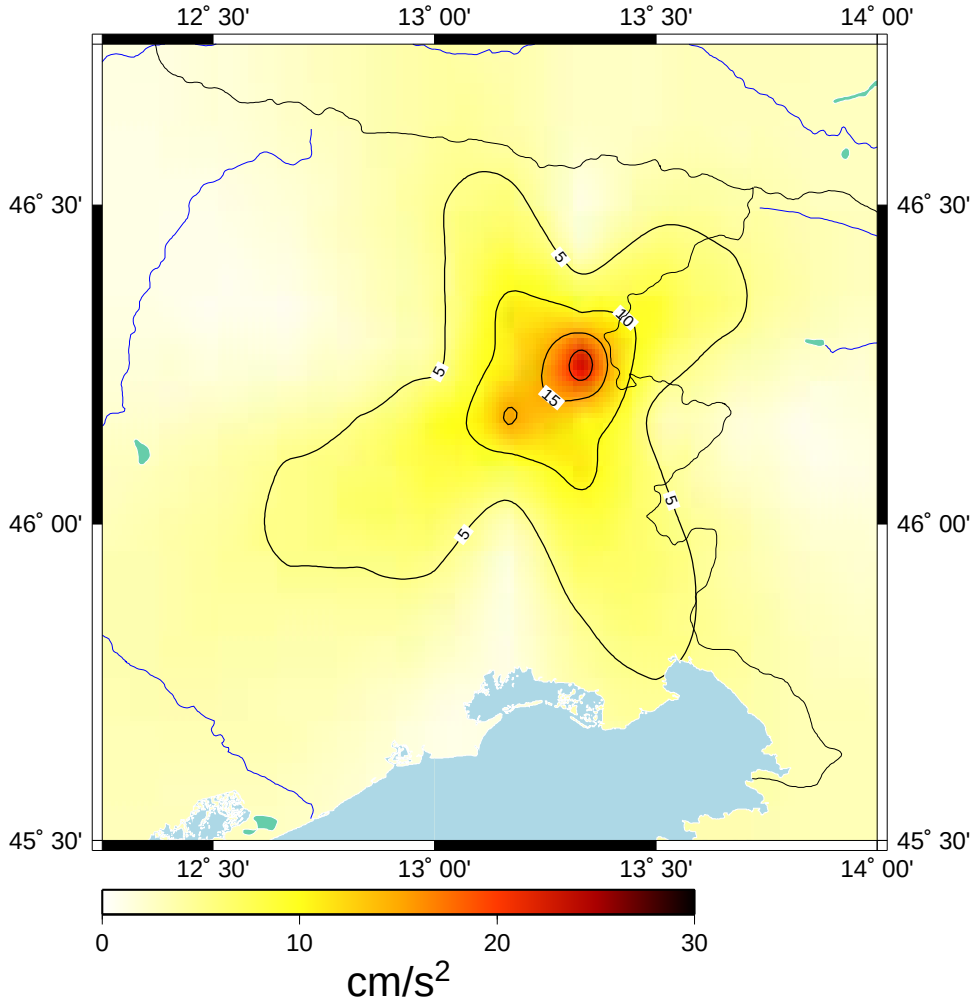

Figure 2.4: Interpolated peak accelerations from Figure 2.3 for the Friuli 1976 event. For the near source area see figure 2.6.

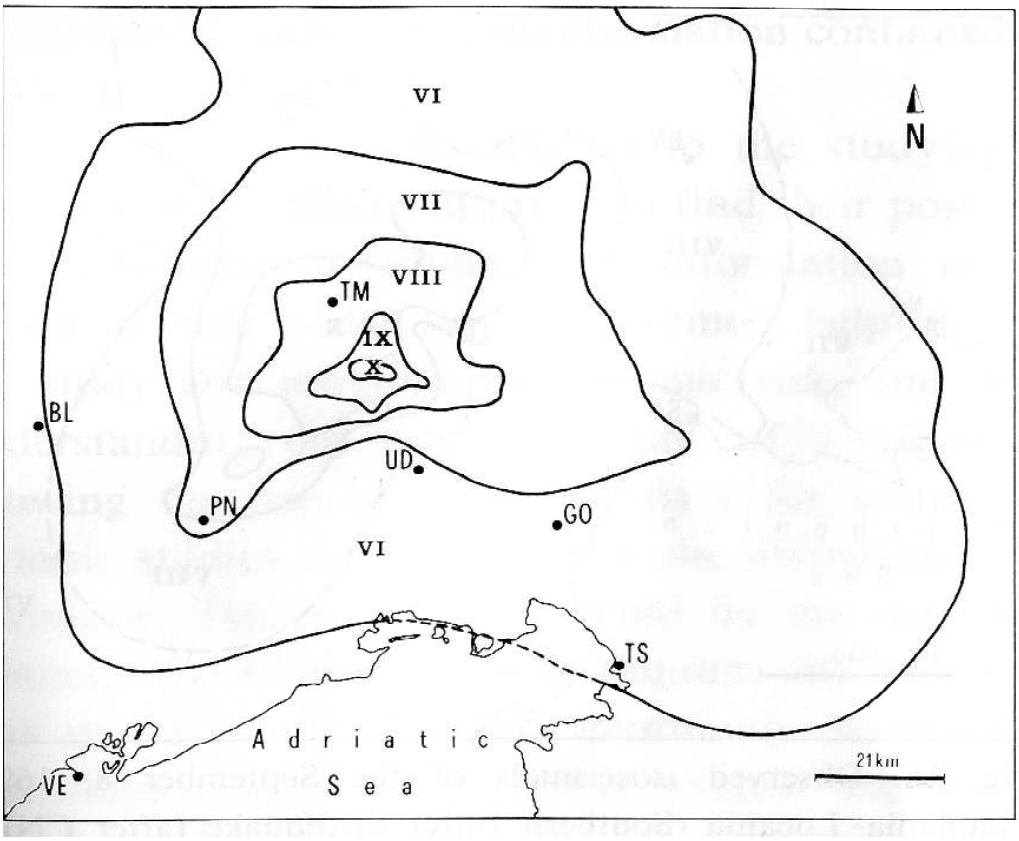

Figure 2.5: Observed macroseismic intensity for the 1976 Friuli earthquake after [Giorgetti, 1976]

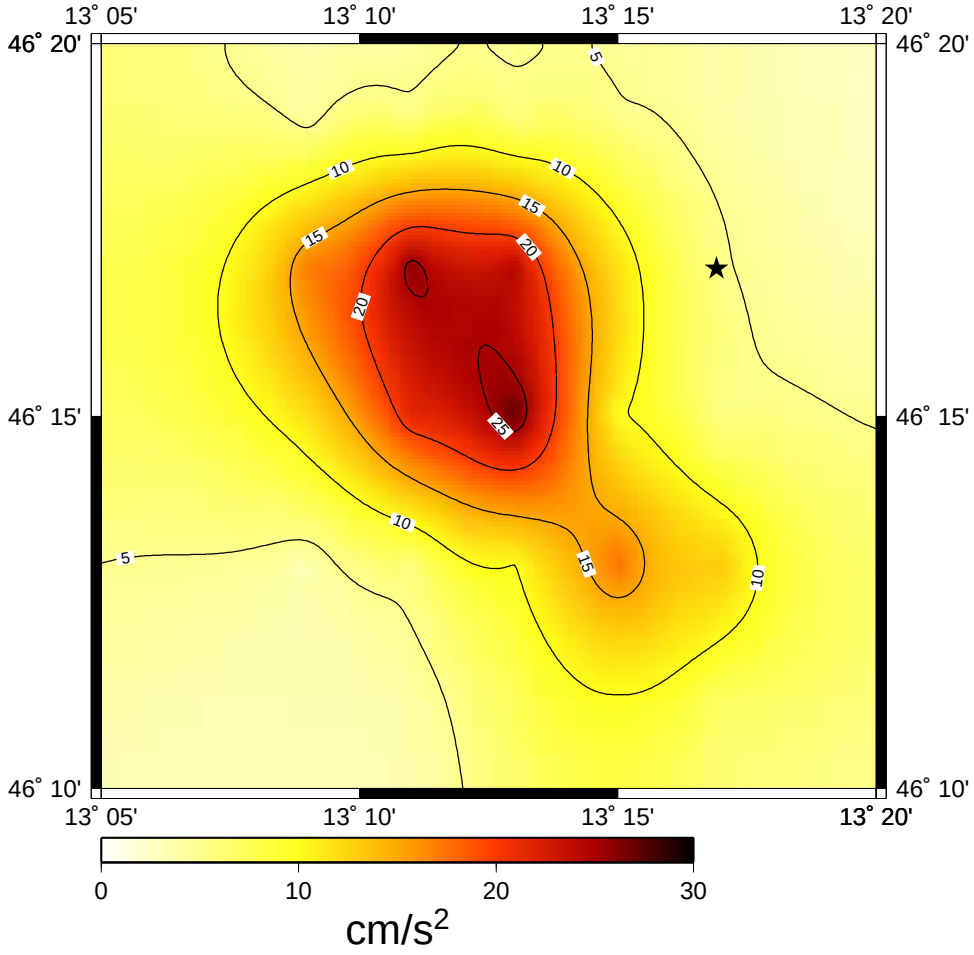

Figure 2.6: Computed peak accelerations (1 Hz maximum frequency)on an equally spaced grid from the source model of Figure 2.2 for the Friuli 1976 scenario, near source area. The star indicates the nucleation point, see Figure 2.1 for reference.

Date	Time	Lat. N	Long. E	M_D	Strike	Dip	Rake	Location
1998/05/28	09:32	46.266	13.117	4.1	102	85	-141	Trasaghis
1998/05/28	09:36	46.185	13.082	3.5	83	82	-144	Trasaghis
2002/02/14	03:18	46.331	13.098	4.9	127	87	117	M. Sernio
2005/12/12	16:35	46.504	13.408	3.3	130	75	163	Pontebba

Table 2.2: Source parameters of events in the Friuli area inverted with waveform modelling

The analyzed recent events in the Friuli area are reported in Table 2.2 and in Figure 2.7. We have chosen only those $M > 3.5$ events that had a good stations coverage. The data used in the inversion comes mostly from the accelerometric stations of the *RAF*. We have two events in the area of Trasaghis (the most southern ones), the Mount Sernio event of February 14, 2002, and a recent small event located near Pontebba.

It is evident that, due to an always growing network, the most recent event waveforms have been inverted for the same parameters in spite of a relatively low magnitude. We have had many similar magnitude events but with a worse azimuthal coverage. The Pontebba event was however the most interesting to study, having occurred in an area of very low recent seismicity near the border with Austria.

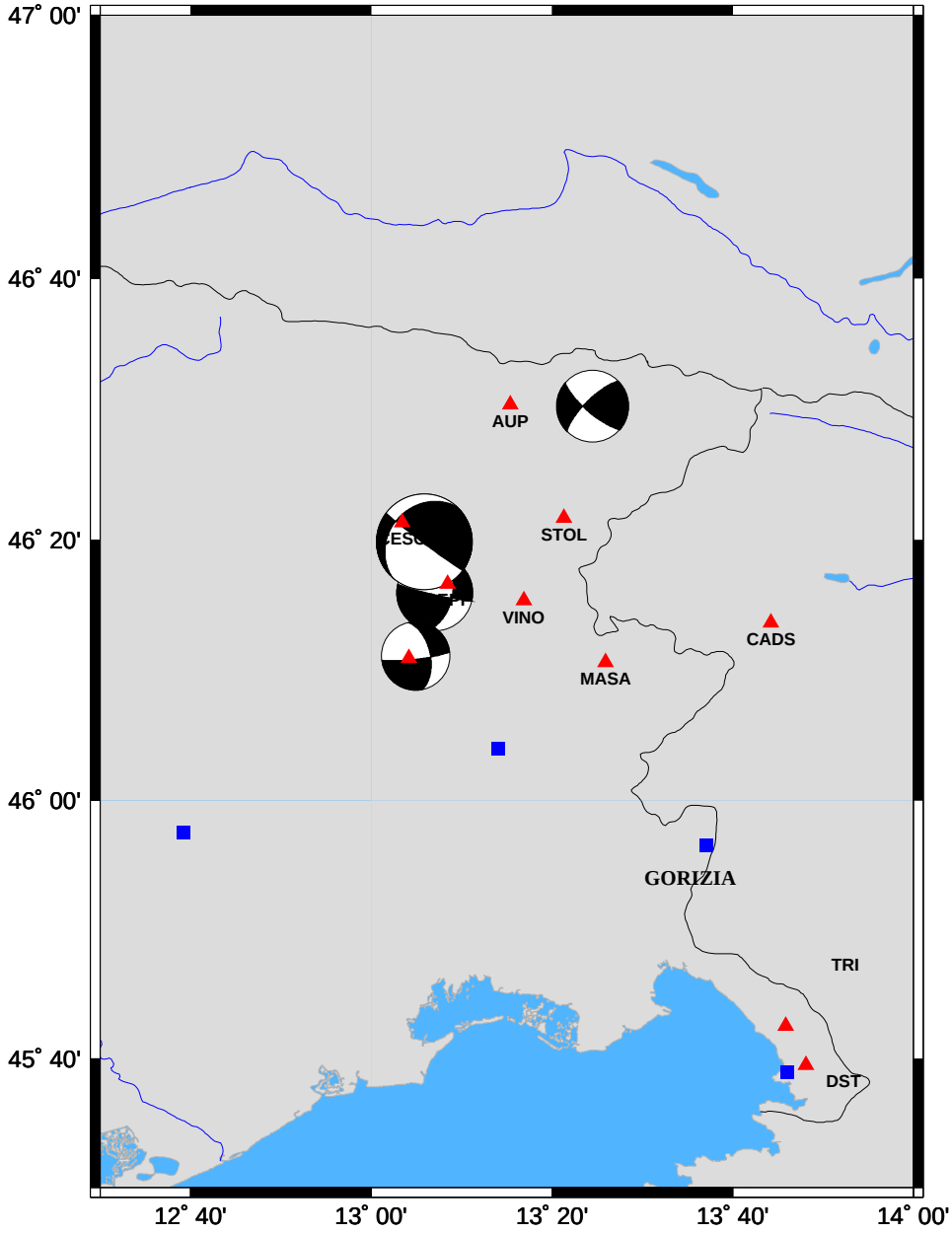

Figure 2.7: Source mechanisms for the major recent events of the Friuli area inverted with waveform modelling (see Table 2.2)

2.4 February 14, 2002 M. Sernio event

As we can see from Table 2.1 this event was one of the strongest to hit the Friuli area since 1976. It is interesting because, since the quality and the number of instruments present in the area has grown up with time, the available digital recordings allow us to perform more detailed studies.

What makes this event even more interesting is that we can model it in the near source region, since we have one strong motion station placed almost above the source. For this reason we have chosen to analyze this event with the reflectivity method which allows us to compute complete and accurate synthetic signals at very short epicentral distance.

2.4.1 The reflectivity method: a quick introduction

The reflectivity method is a method to compute synthetic seismograms. Its main characteristics are a good modelling of body waves at small source receiver distances. The method is based on the computation of the reflectivity coefficients of the layers of the 1D model, hence its name. Afterwards an integration in the slowness domain is performed, following [Kennett, 1983].

The signals in the frequency domain are displacements, to obtain velocities we need to differentiate the signals. This is easily done in the frequency domain multiplying the related spectra by $-i\omega$. For a more detailed explanation of the method see Appendix A.1.

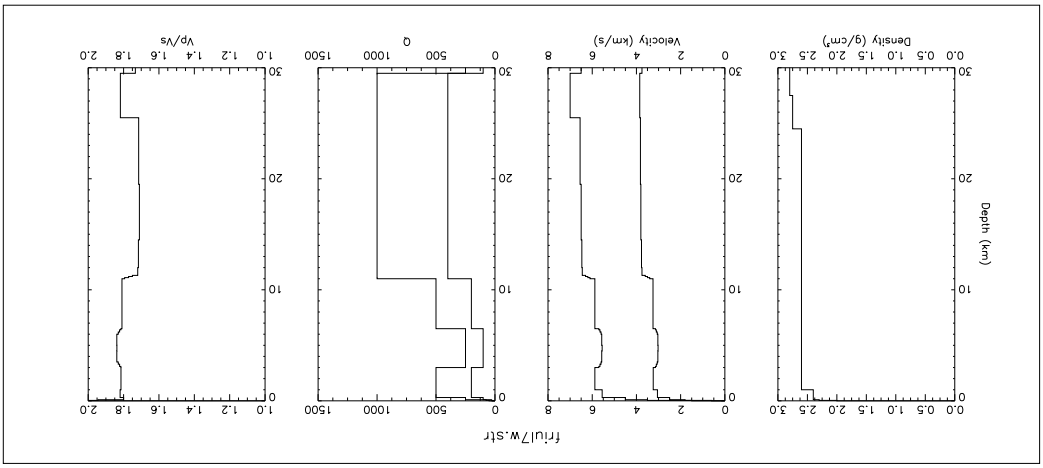

Figure 2.8: The velocity model used for the tests, Friul7w [Costa et al., 1993].

2.4.2 Finite source modelling in the near source

The Department of Earth Sciences of the University operates a strong motion network, the RAF (Rete Accelerometrica del Friuli). In its database it is possible to find many events, of various magnitude, and recorded at various distances. For testing the reflectivity code we have implemented in the framework of this thesis we have chosen the event of February 14, 2002, located in the area near Moggio Udinese (UD), almost at the geographical center of the network. We have mainly used the data from the stations MOGG and CESC, both at less than $10km$ from the epicenter, but also the data from many other stations at farther epicentral distances, the latter mainly for the source inversions and for a reference.

The structural model used is the one represented in Figure 2.8, the Friul7W structure [Costa et al., 1993], the location is the one provided by CRS-INOGS, and the source mechanism is the one proposed by the internet

database of ETHZ [ETHZ, 2006]. We have chosen the location from OGS thanks to its usage of near station that should make it more accurate, while the source mechanism from Ethz has been chosen due to a better azimuthal coverage.

The location chosen is 13°06′00″ East and 46°25′30″ North, with a main nodal plane with a strike of 322°, a dip of 26° and a rake of 197°. The epicenter is plotted relatively to the location of the recording stations. The fault model used has an uniform slip and a size of $2km \times 2km$

The agreement between synthetics and data is fairly good. When working with such a small epicentral distance the accuracy of the velocity model becomes crucial.

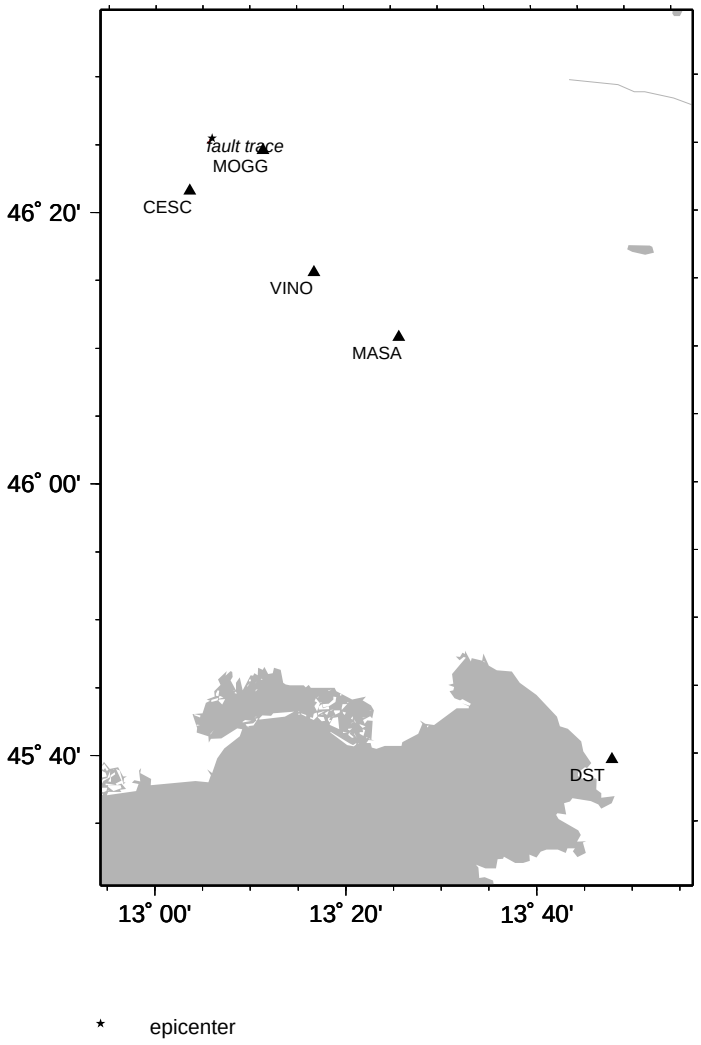

Figure 2.9: Fault position and stations used for the Mt. Sernio 2002 event forward modelling

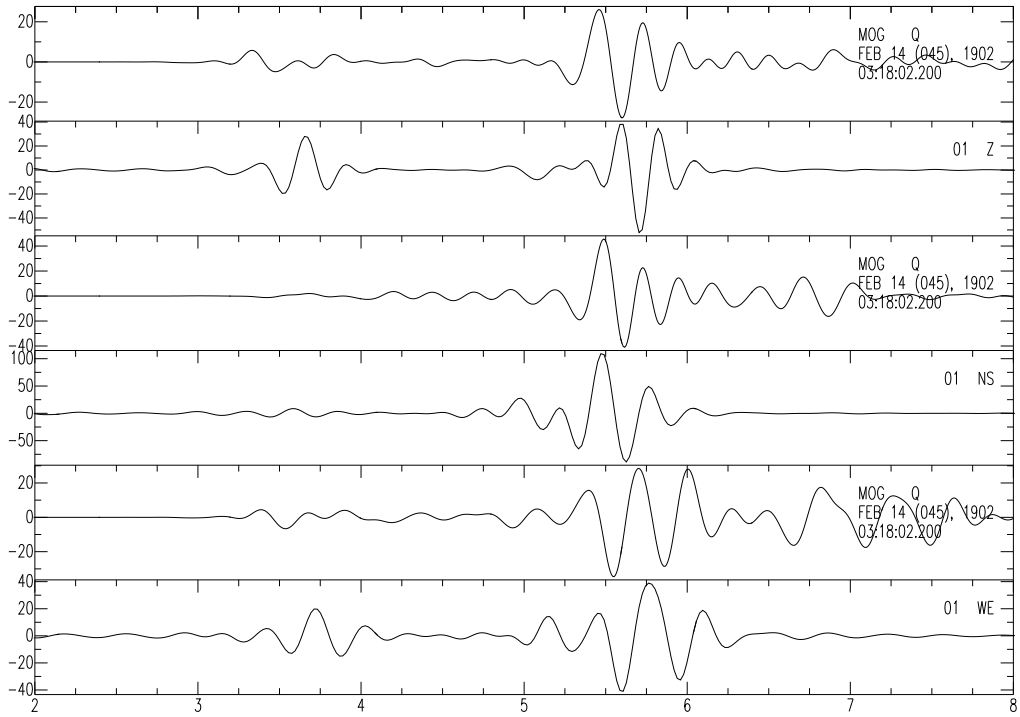

Figure 2.10: Data and synthetic seismograms, LP 5Hz for the MOGG station

Chapter 3

The Bovec Area

3.1 The area

3.1.1 Recent seismicity

We will focus on this area, that has been recently hit by a $M_W = 5.6$ earthquake on April 12, 1998 and by a $M_W = 5.2$ earthquake on July 12, 2004, both with their series of aftershocks.

3.1.2 Seismic sources

Some previous studies [Aoudia, 1998] have delineated which are the active faults of the area (Figure 1.1). The Bovec Area, subject of our study, belongs to the Northern area characterized by strike slip faults, while having the first thrust faults appear further to the west.

3.1.3 1998 sequence

The 1998 sequence has been extensively analyzed in another previous study [Bajc et al., 2001]. The fault plane has been identified by JHD relocation of the sequence and the magnitude of the main event has made reasonable to try also a finite source inversion of the event.

The noticeable characteristics of the 1998 sequence are a fault plane oriented $NW - SE$ with a slight bifurcation north. The moment release is concentrated in the area between 5 and 7 km deep.

Most of the study of the 1998 sequence comes from previous studies [Bajc et al., 2001], we have considered it mainly in its relationship with the 2004 sequence.

3.1.4 2004 sequence

Distribution in time

The first thing to note, directly from unrelocated aftershocks, is the time distribution of aftershocks. We can see in it Figure 3.1. According to Omori's law [Lay and Wallace, 1995] the decay in time should follow an inverse proportionality law.

$$n = \frac{C}{(K+t)^P} \tag{3.1}$$

where n is the frequency of aftershocks at time t after the mainshock, K, C and P are parameters that depend on the size of the earthquake.

This is a moderate size earthquake, and so after some times the amount

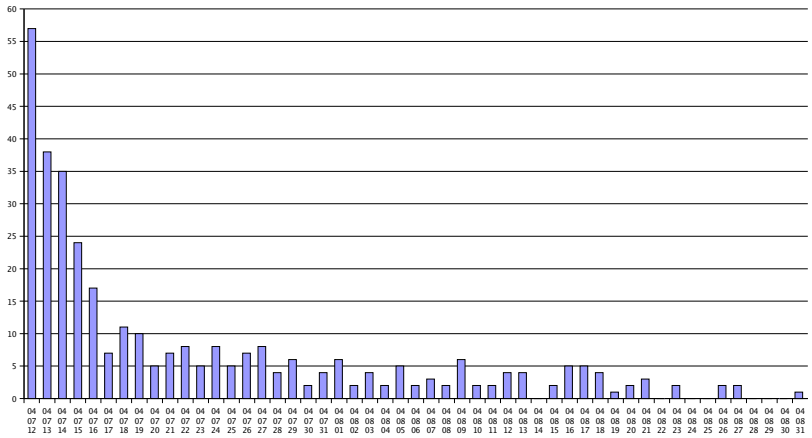

Figure 3.1: Time distribution of relocated aftershocks

of aftershocks relocated that can be considered decreases greatly. So it makes little sense to perform further statistical analysis.

Distribution in space

The 2004 sequence has been characterized by a local network much denser than that in operation during the 1998 sequence. The obtained absolute locations are thereafter more accurate, even if some questions remain about the relative location of the 1998 and 2004 sequences. This can be seen from Figure 3.5 where the epicentral view of the two sequences are plotted.

In Figure 3.6 we can see the sequence along a cross section perpendicular to the fault. The picture is taken with an orientation of 120° degrees north, according with the estimates of the focal mechanism obtained from waveform inversion and with the seismotectonics of the area. This picture gives us a rough estimate of the quality of the relocations, since the clusters are well

packed.

In Figure 3.7 we can see how the rupture evolved. On the left we can see the 2004 events (in cyan) while on the right we can see the 1998 events (in orange). The image is heading 30° north. In 2004 the 1998 rupture evolved towards the north-west, while the aftershocks have been all shallower than the main shock.

Various relocations have been performed, relocating in a joint inversion both sequences or relocating each sequence separately. The separate relocation showed a strong bias and a difference in epicentral location of more than 2 km (see Figures 3.5 and 3.2).

3.1.5 Joint or separate relocation?

When performing the JHD inversion we were faced with a question: the two sequences should be considered as a single one or as two different events? The first approach looks more reasonable, the two events being very close in space, but we have to consider: the common base of stations between the two sequences is rather small. Most of the permanent stations in the area have been placed after the 1998 sequence and few of the temporary station have retained their locations until 2004. Also, to enhance the location for the 1998 sequence it has been necessary to use regional phases, while for the 2004 sequence this was not necessary, due to the greater number of available local stations.

We have performed some tests with both the configurations. Considering the 1998 and the 2004 sequences jointly reduced the relative distance between

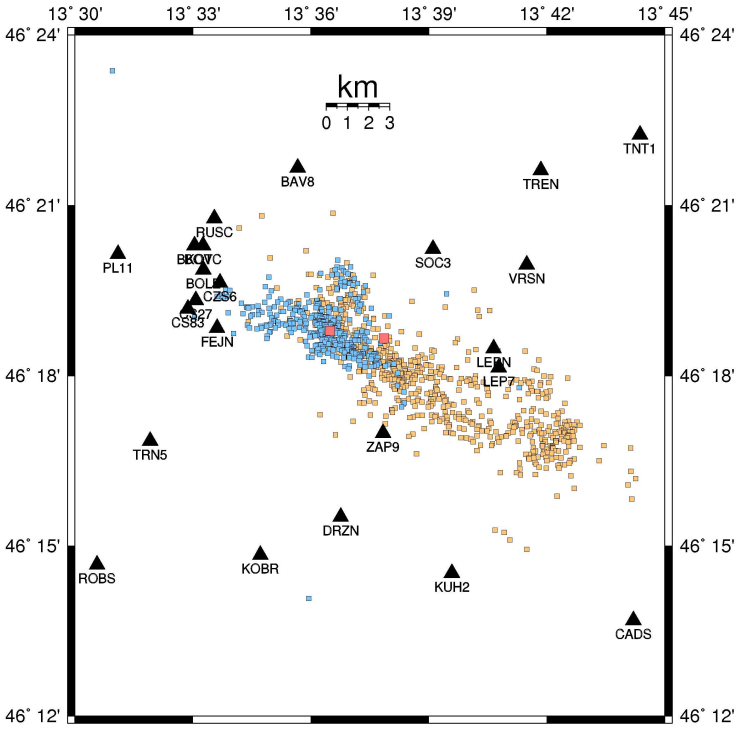

Figure 3.2: 1998 (orange) and 2004 (cyan) sequences (main shocks in red) epicentral view: joint relocation

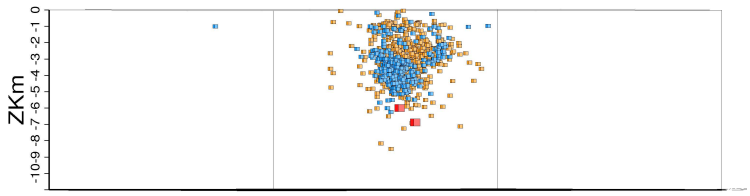

Figure 3.3: 1998 (orange) and 2004 (cyan) sequences (main shocks in red) transverse fault view: joint relocation

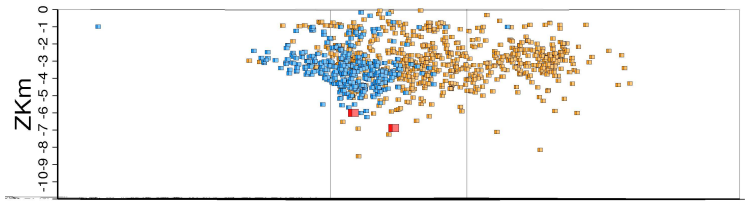

Figure 3.4: 1998 (orange) and 2004 (cyan) sequences (main shocks in red) perpendicular fault view: joint relocation

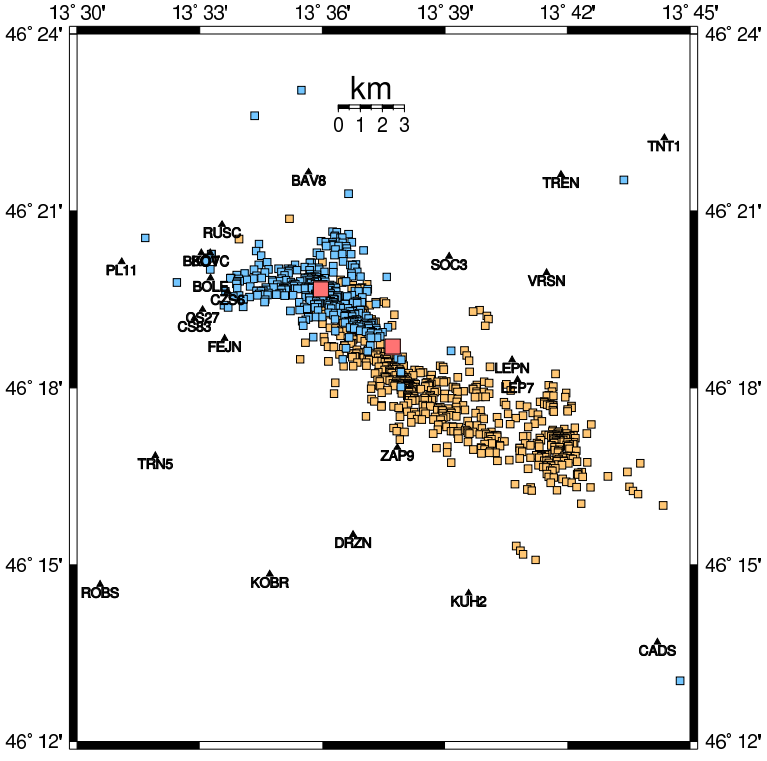

Figure 3.5: 1998 (orange) and 2004 (cyan) sequences (main shocks in red) epicentral view: two separated relocations

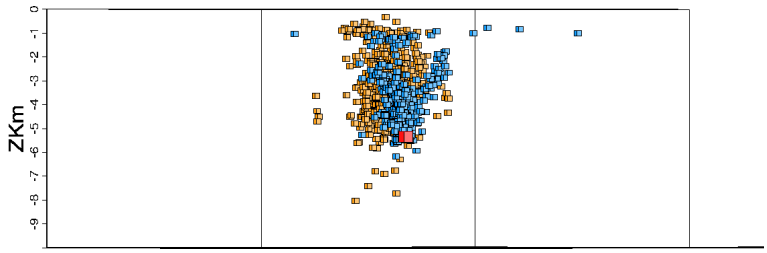

Figure 3.6: 1998 (orange) and 2004 (cyan) sequences (main shocks in red) transverse fault view: two separated relocations

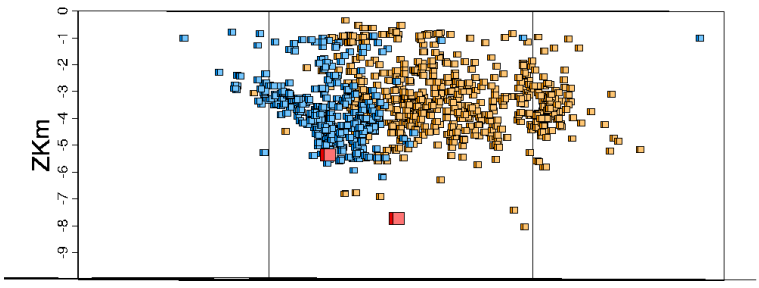

Figure 3.7: 1998 (orange) and 2004 (cyan) sequences (main shocks in red) perpendicular fault view: two separated relocations

the main events and their aftershock sequences, while reducing slightly the tightness of the locations of the 2004 sequence.

The solution we are willing to accept is the joint relocation one, mostly because of the location of the 2004 cluster. From active tectonics the fault is not supposed to be as north as it would be located by the separate location, since that would place it just below Bovec valley, thus making little sense from a tectonic point of view.

Also the recordings of some local station suggest from $P-S$ pickings and polarities that the event is possibly located near to the 1998 event earthquake, since waveform the similarities in the recordings of both the main events is striking [Živčić, personal communication].

3.2 Source parameter inversion

The 1998 event has been already studied previously [Bajc et al., 2001]. We will perform the inversion only for the 2004 event.

3.2.1 Method and input data

In this study we will perform source parameters inversion the method proposed in the Appendix C.1 [Mao et al., 1994] [Delise, 2003]. The data comes out of the joint broad band network, developed in the framework of the Project Interreg III A *Reti sismologiche senza confini nelle Alpi Orientali* [Bragato et al., 2003], with data coming from Austria, Slovenia, and Italy.

The trial solution, necessary for this kind of inversion, has been taken

from the Mednet catalogue [Mednet, 2006].

3.2.2 Results

The method is a linearized one. So we are always at risk that our solution is not the absolute minimum of residuals, but only a local minimum. To overcome this limitation we need to perform different inversions with different trial solutions. The results are rather stable, showing a source mechanism characterized by a strike, dip and rake, respectively, of 124°, 87° and 171°. The result is compatible with the fault plane identified by the aftershock relocation.

3.3 Stress Analysis

3.3.1 Coulomb stress analysis

The Coulomb stress analysis is based on the studies of Amonton in 1699 and Coulomb in 1773. The idea is that the shear strength of a rock, $|\tau|_{failure}$, is equal to a constant plus a factor proportional to the normal stress σ_n on the plane. The result of these studies is the so called *Coulomb failure criterion*

$$|\tau|_{failure} = c + \mu_i \sigma_n \tag{3.2}$$

where c is the strength of the rock, μ_i is the so called constant of internal friction [Scholz, 2002].

To compute the stress distribution due to a fault in an earth model is an elastostatics problem for which, in the case of an half space a complete set of

closed analytical expressions is available for strain and its derivatives. Since the expressions are rather huge, and they have already been implemented in the software we refer to literature for further reference [Okada, 1992].

In particular, we are interested in a finite rectangular fault and stress distribution, which means we need to obtain stresses from strains using

$$\sigma_{ij} = \lambda \frac{\partial u_k}{\partial x_k} \delta_{ij} + 2\mu \frac{1}{2} \left(\frac{\partial u_i}{\partial x_j} + \frac{\partial u_j}{\partial x_i} \right) \tag{3.3}$$

3.3.2 Data and model used

For the source of the 1998 event we have used a simplified model based on the proposed finite source [Bajc et al., 2001]. This model was obtained from surface waveform modeling, allowing a fine resolution of the moment distribution on the fault. For our needs, however, it was enough to divide the fault in six rectangular subfaults, of known moment and area.

The model used has a strike of 315°, a dip of 82° and a rake of −171° with a total seismic moment of $4.5 \times 10^{17} Nm$. The seismic moment has been concentrated on the central zone at higher depths and near the surface at the two ends of the fault, while leaving a constant moment density of $5 \times 10^{15} \frac{Nm}{km^2}$.

Adding a fine moment distribution on the fault, however, does not give very significant differences from the uniform slip model. We can see it comparing Figure 3.8 and Figure 3.9. So for the second event, since we do not have a slip distribution on the fault, we can confidently consider a uniform slip model.

For the 2004 event we have performed a waveform inversion for source parameters [Mao et al., 1994][Delise, 2003] using data from the North-Eastern

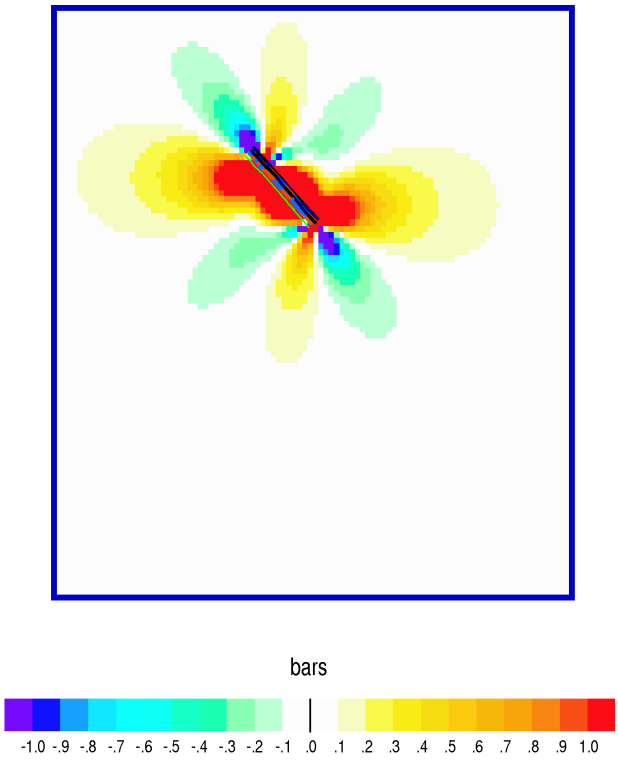

Figure 3.8: Coulomb stress change due to the 1998 earthquake modeled with a finite fault with uniform slip

Italy (NI) broad-band network, the Slovenian and the Austrian network. We have then used empirical relations [Wells and Coppersmith, 1994] to infer finite source dimensions, obtaining a source area of $4 \times 4km$.

For this event we have considered a strike of 124°, a dip of 87° and a rake of 171°, with a seismic moment of $4.9 \times 10^{16} Nm$.

We have added a regional stress field too, with the principal axis oriented North - South [Bressan et al., 1998]. It must be kept in mind, however, that the amplitude, not reported, hardly matters [King et al., 1994] so we assume it to be around 15 bars.

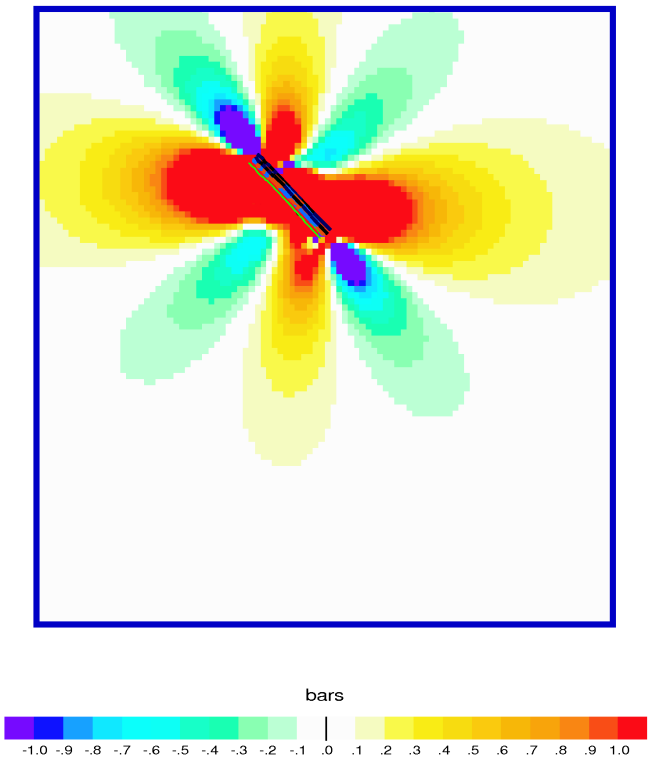

Figure 3.9: Coulomb stress change due to the 1998 earthquake modeled with the finite source model [Bajc et al., 2001]

The elastic properties of the model are taken from the structure Friul7w [Costa et al., 1993], obtained from P-wave arrival times inversion. Since we can model stress for an half space, we have considered in the analysis the characteristics of the structure at the computation depth of $5.0km$, a recurrent depth for earthquakes in the area..

From the performed catalogue analysis we can assume a similar behavior under stress of all the area, allowing us to use the 1D approximation in modelling.

3.3.3 Coulomb stress field

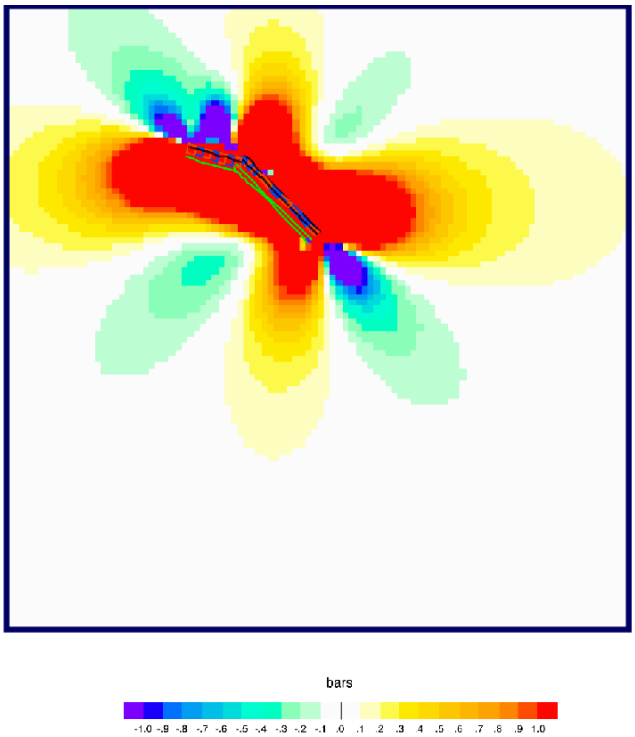

Figure 3.10: Coulomb stress change due to the joint effect of the 1998 and 2004 earthquakes.

From Figure 3.9 we can establish a connection between the 1998 and the 2004 earthquakes. We can see that the 2004 fault resides in an area for which the 1998 event has increased the Coulomb stress, increasing the possibility of an earthquake on the active faults present in this area.

Figure 3.10 gives the situation after 2004 event. It raised once more the stress on the area just west and east of its fault trace. While there is hardly any evidence of active faults east of the Bovec events (even if there should be some on the basis of general tectonic considerations), west of them we have

some thrust faults that could be activated in the near future.

From this model we could expect that the rupture should not continue further south on the fault, stopping at the Tolminka spring basin, while we could expect an earthquake on the thrust faults located between the area to the west of Bovec, towards Italy, and the area struck by the destructive earthquake in 1976 [Aoudia et al., 2000], or to the area East of Bovec.

For the Friuli 1976 event and aftershocks a similar study has been already carried out [Perniola et al., 2003] showing the applicability of this method in this area.

Chapter 4

Seismicity and fault mechanisms of recent events in other seismic areas of western Slovenia

4.1 Podbrdo area

On 14/01/2005 two consecutive events hit the area of Podbrdo, 15 km East-South-East of Bovec. The previous studies makes us link it with the Bovec area, since the stress redistribution due to 1998 and 2004 may have triggered this event.

The event has been located by the Slovenian Seismic Network operated by ARSO.

Date	Time	Lat. (N)	Long. (E)	M_l	Strike (degrees)	Dip (degrees)	Rake (degrees)
2005/01/14	07:58	46.168	13.968	4.1	250	78	0
2005/01/14	08:05	46.170	14.015	3.9	17	87	-14

Table 4.1: Source parameters of the events in the Podbrdo area inverted with waveform modelling

4.1.1 Source parameters waveform inversion

These were small events, with $M = 4.1$ and $M = 3.9$. So, unlike for the previous, it has been impossible to find a reliable trial solution. So we performed different inversions with different trial solution, with the most common source mechanisms of the area. Both reached a stable solution, showing a decent stability of the algorithm, with only minor differences on the final depth result of the inversion. For the results, see Table 4.1.

The inverted mechanisms are plotted in detail, together with Bovec 2004 event, in Figure 4.1

4.1.2 Relation with Bovec events

From Figure 3.10 we can see an increase of Coulomb stress on the areas South-East and North-West of Bovec. Podbrdo is sited South-East of Bovec, in an area of increased stress.

So we can say there is a link between the two events. We could even dare express it as a cause-effect relationship between the two sequences. This is

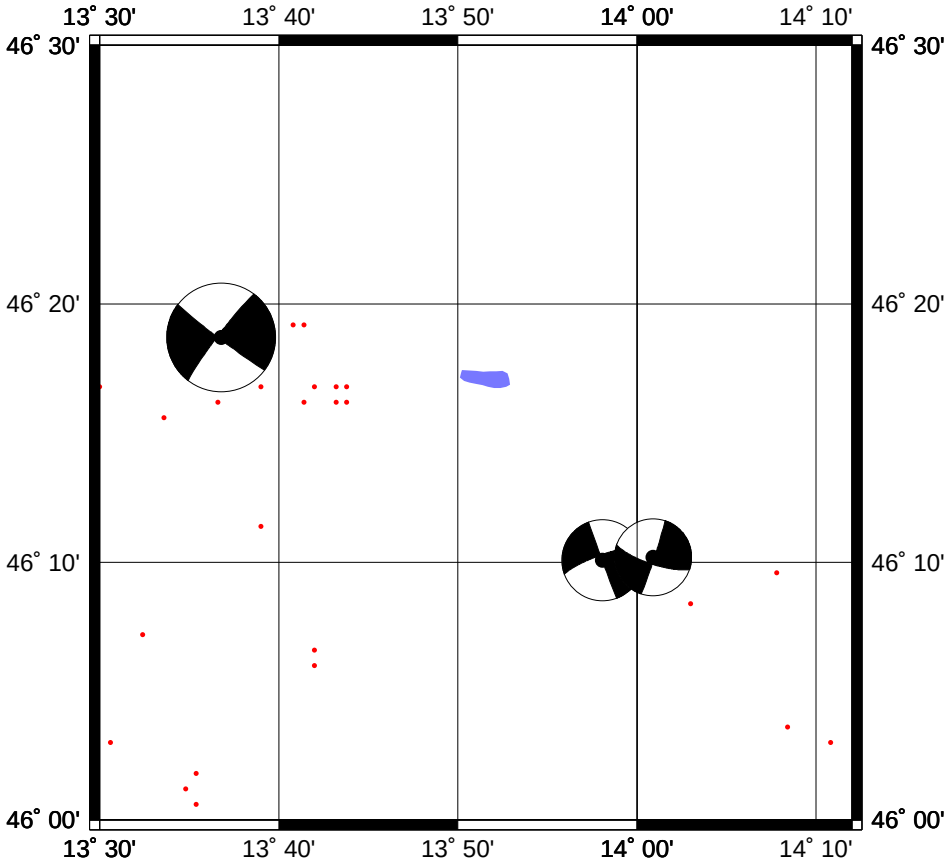

Figure 4.1: Source mechanisms of Podbrdo area events with, in red, historical seismicity with $M > 3.5$

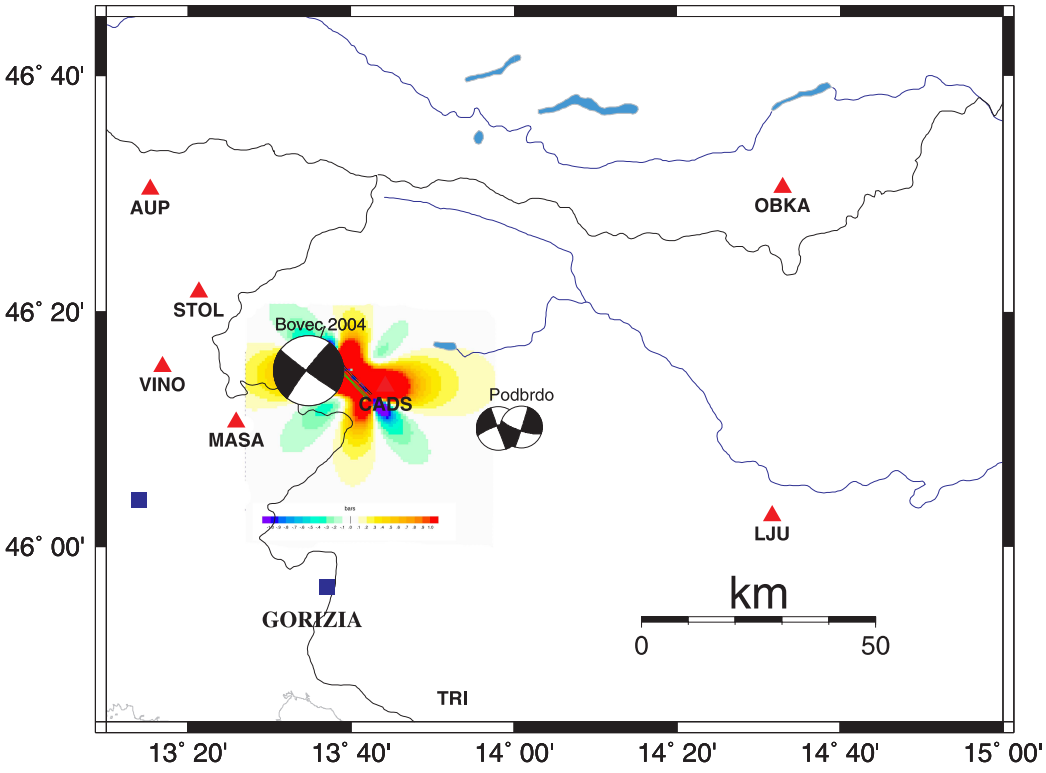

Figure 4.2: Podbrdo and Bovec events plotted together with Coulomb's stresses

much clearer from Figure 4.2.

The link has come much to our attention since the study of the Coulomb stress has been performed just after July 2004 and well before January 2005.

4.2 Mount Snežnik and the Dinarides area

From a seismotectonic point of view, the area of mount Snežnik is located in south-western Slovenia, on one of the long transform fault, the Raša - Cividale which is parallel to the Idrija one [Aoudia et al., 2000].

Date	Time	Lat. (N)	Long. (E)	M_l	Strike (degrees)	Dip (degrees)	Rake (degrees)
1998/02/04	14:07	45.506	14.472	3.5	338	86	175
1998/03/13	15:14	45.605	14.211	4.2	160	81	169
1998/06/02	20:46	45.820	14.049	3.0	311	89	-178
2002/06/02	13:37	45.615	14.241	3.8	333	84	-178
2005/04/24	18:33	45.601	14.352	4.2	142	84	173
2006/06/21	06:18	45.387	14.474	3.6	332	82	-176
2006/08/07	04:59	45.187	14.753	3.7	317	64	170

Table 4.2: Source parameters of events in the Sneznik area, inverted with waveform modelling

4.2.1 Recent seismicity

The area has recently been hit by some moderate size earthquake ($M_l <$ 4.5). The most recent ones (1998 - 2002) have been felt in a rather wide area, up to the center of Trieste, amplified by the soft soil of the centre of the city [Fitzko et al., 2007]. This is one of the nearest seismogenetic areas of Trieste.

The mechanisms obtained (see Table 4.2 and Figure 4.3) are in good agreement with previous studies [Herak et al., 1995]. Not surprisingly, they are compatible with a structure of transcurrent faults oriented more or less 120° from north. In this they agree also with seismotectonic studies [Aoudia, 1998]

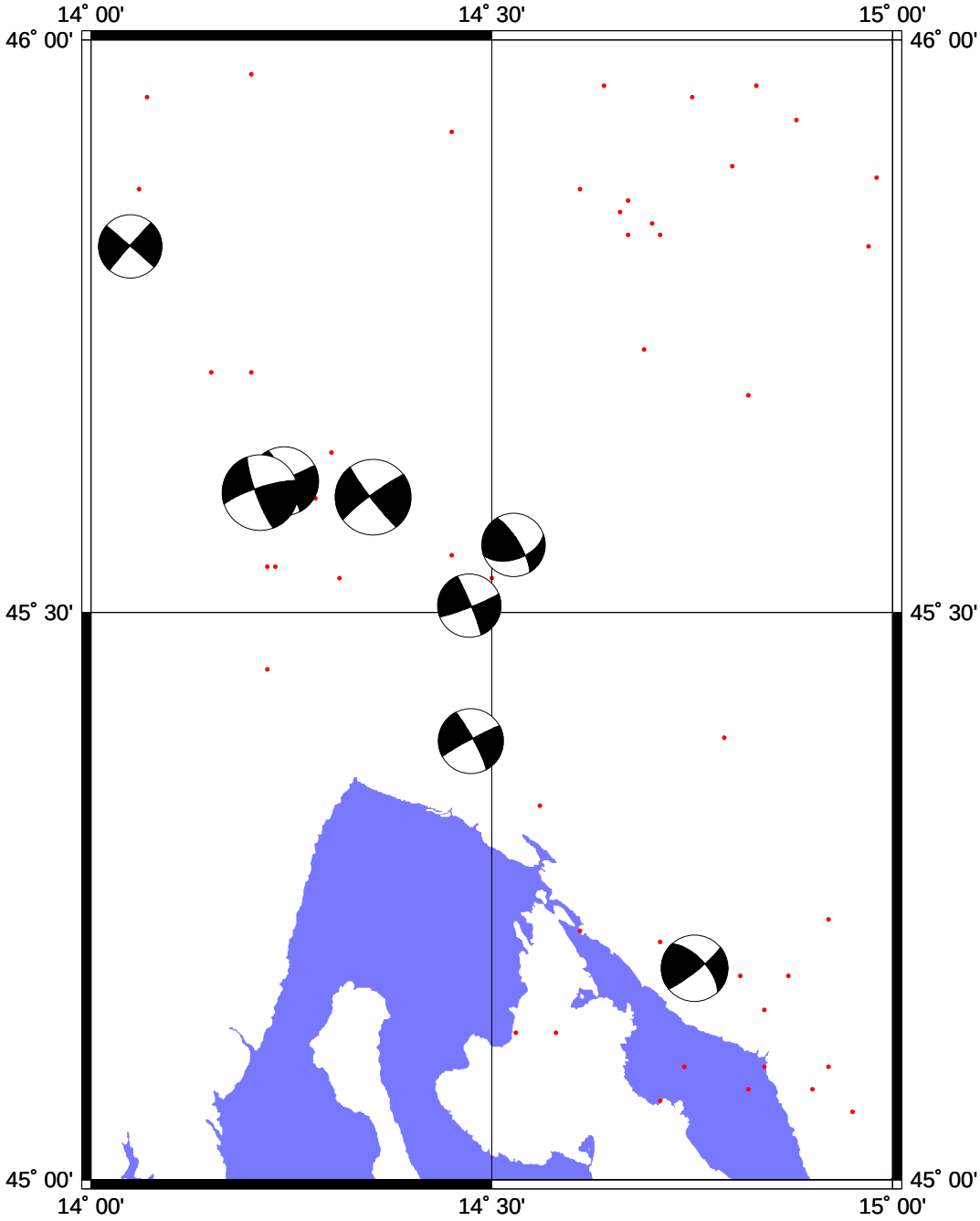

Figure 4.3: Source mechanisms of Sneznik area events with, in red, historical seismicity with $M > 3.5$

4.3 Overview of the area

From all this source mechanisms (see Figure 4.4) obtained we can have an overview of the area. The mechanisms mainly agree in defining a stress field oriented north-south. We can recognize the main tectonic characteristics of this area, the transcurrent faults oriented NW-SE.

The Podbrdo area, while being out of the transcurrent faults area, shows however source mechanisms compatible with the stress field.

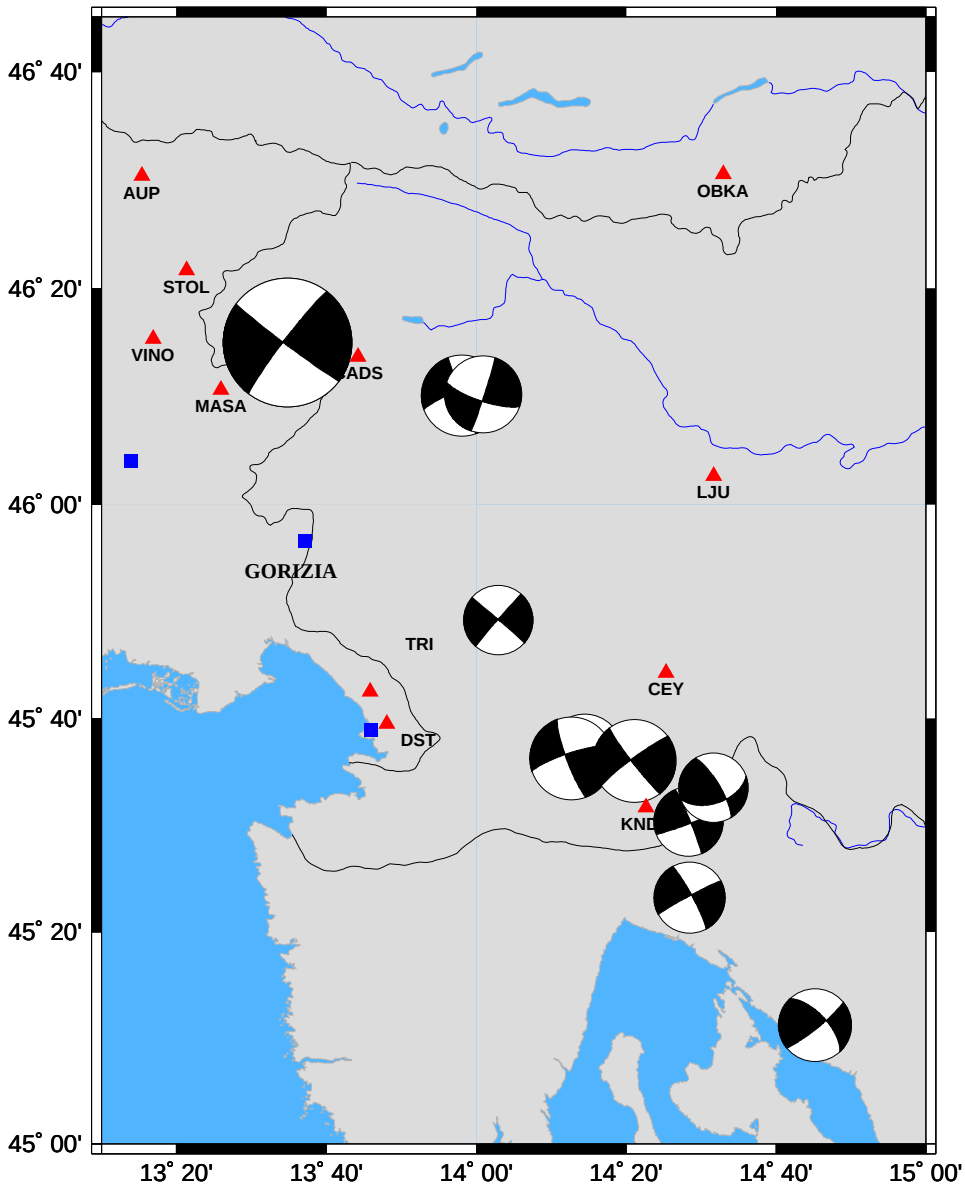

Figure 4.4: Source mechanisms for the major recent events of the Slovenian area (see Table 4.1 and 4.2)

Chapter 5

Conclusions

In this study we have adapted the reflectivity method package developed for applied geophysics purpose [Kennett, 1983] to obtain synthetic seismograms related to earthquake signals, in particular for what it concerns the extended source modelling, and we have applied it to study the Friuli area events. In particular, to validate the method, we have performed both the direct modelling of the 2002 Carnia event, obtaining for it a $2km \times 2km$ fault area, and calculated a scenario for the Friuli 1976 event, which turns to be compatible in its pattern with the observed macroseismic intensity felt.

In the second part we have performed a JHD relocation for the 2004 Bovec sequence, comparing the aftershock relocations with those related to the 1998 sequence. We have observed that the 1998 rupture continued towards NW during the 2004 event. This is in agreement with the post event Coulomb's stress distribution [Toda and Stein, 2002], obtained by modelling the 1998 Bovec event. From the Coulomb stress modelling we recognize also a general

increase of stress to the West and to the East of Bovec epicentral area.

At last we have performed a waveform source parameter inversion for four events in the Friuli area and eleven events in the Western Slovenia area (magnitude mainly $M > 3.5$), finding fault plane solutions in agreement with both the North-South directed stress field and the geometry of faults in each of the areas.

Appendix A

Synthetic seismograms with the reflectivity method

A.1 Synthetic seismograms

A.1.1 The problem

The complete analytical solution of the seismic wavefront due to a seismic source in a multilayered earth is not possible. So we have to use either a numerical method, or an approximation. The reflectivity method belongs to the first category. The numerical integration can be carried out in the horizontal wavenumber [Fuchs and Müller, 1971] or in the slowness domain [Kennett and Kerry, 1979].

In this study we will follow the approach of [Kennett, 1983]. The principle upon which the reflectivity method is based is rather simple: we need to compute reflection coefficients for upgoing and downgoing waves as a function

of slowness, integrating over slowness and finally applying a convolution with the source function.

A.1.2 The solution

First of all we need to define a stress displacement vector $\mathbf{b}$ function of k (wavenumber), m (azimuthal order), z (depth) and ω defined as follows

$$\mathbf{b}(k, m, z, \omega) = [\mathbf{w}, \mathbf{t}]^T \tag{A.1}$$

where $\mathbf{w}$ is the displacement vector and $\mathbf{t}$ is the traction vector.

We represent the source as a discontinuity in the stress-displacement vector at the source depth z_S. That is

$$\mathbf{b}(z_S+) - \mathbf{b}(z_S-) = \mathbf{S}(z_s) \tag{A.2}$$

We need then to force, for the deepest layer (the half space, for $z > z_L$) the condition of no-upward radiation, that is to exclude upgoing waves by taking

$$\mathbf{b}(z_L) = \mathbf{D}(z_L)[\mathbf{0}, {}_D]^T \tag{A.3}$$

$\mathbf{D}$ is the eigenvector matrix and c_D are downgoing wave elements which will depend on properties of the source and the half space. We need then to obtain the stress-displacement vector as a function of the stress displacement vector at the source layer. To do so we need to define the propagator matrix $\mathbf{P}(z_S, z_L)$ [Gilbert and Backus, 1966] with

$$\mathbf{P}(z, z_0) = \mathbf{B}(z)\mathbf{B}^{-1}(z_0) \tag{A.4}$$

where $\mathbf{B}$ is the matrix of the displacements and stresses, defined as

$$\mathbf{B} = \begin{pmatrix} \mathbf{W}_{UG} & \mathbf{W}_{DG} \\ \mathbf{T}_{UG} & \mathbf{T}_{DG} \end{pmatrix} = \begin{pmatrix} \mathbf{b}_{UG} & \mathbf{b}_{DG} \end{pmatrix} \tag{A.5}$$

where $\mathbf{W}$ are the displacement matrices, and $\mathbf{T}$ are the traction matrices. The index $_{UG}$ indicates the upgoing radiation, while the index $_{BG}$ indicates the downgoing radiation.

We apply then the propagator matrix to the downgoing wave, obtaining the $\mathbf{b}$ vector just below the source

$$\mathbf{b}(z_S+) = \mathbf{P}(z_S, z_L)\mathbf{b}(z_L) \tag{A.6}$$

and from Equation A.2 we can obtain the field above the source, that is

$$\mathbf{b}(z_S-) = \mathbf{P}(z_S, z_L)\mathbf{b}(z_L) - \mathbf{S}(z_S) \tag{A.7}$$

Then we can apply the propagator matrix to the vector over the source up to the free surface. Using the propagator chain rule, we can obtain

$$\mathbf{b}(0) = \mathbf{P}(0, z_S)\{\mathbf{P}(z_S, z_L)\mathbf{b}(z_L) - \mathbf{S}(z_S)\} = \mathbf{P}(0, z_L)\mathbf{b}(z_L) - \mathbf{P}(0, z_S)\mathbf{S}(z_S) \tag{A.8}$$

and from it we can obtain the surface displacement at the surface, that is

$$[\mathbf{w}_0, \mathbf{0}]^T = \mathbf{P}(0, z_L)\mathbf{D}(z_L)[\mathbf{0}, \mathbf{c}_D]^T - \mathbf{S}(0) \tag{A.9}$$

The relation between $\mathbf{w}_0$ and $\mathbf{c}_D$ is thus controlled by

$$\mathbf{B}_V L(0) = \mathbf{P}(0, z_L)\mathbf{D}(z_L) \tag{A.10}$$

We can express the source displacement also it in terms of the partitions of $B_V L$ writing

$$\begin{pmatrix} \mathbf{w}_0 \\ -- \\ \mathbf{0} \end{pmatrix} = \begin{pmatrix} \mathbf{W}_U L & | & \mathbf{W}_D G \\ ----- & - & ----- \\ \mathbf{T}_U G & | & \mathbf{T}_D G \end{pmatrix} \begin{pmatrix} \mathbf{0} \\ -- \\ \mathbf{c}_d \end{pmatrix} - \begin{pmatrix} \mathbf{S}_W 0 \\ -- \\ \mathbf{S}_T 0 \end{pmatrix} \tag{A.11}$$

This is the propagation term in the slowness/frequency domain. To recover the full time response we must invert the transforms, and add the source terms.

For the vertical component, for example, we can express it as

$$u_z(r, \phi, t) = \sum_m \int_{\omega_1}^{\omega_2} d\omega \omega^2 \int_{p_1}^{p_2} dp U(p, \omega) S(z_s, m) J_m(\omega p r) e^{\imath m \phi} \tag{A.12}$$

where $U(p, \omega)$ is the propagation term, that does not depend on the angular term m, while this resides in the source term $S(z_s, m)$.

A.2 The implementation of the method

A.2.1 Technical details

The code, kindly provided by prof. B. L. N. Kennett, was written in Fortran 77 in the 80's, so the first step has been to modify it to take full advantage of modern hardware and to have the possibility of obtaining complete seismograms with a single run, without the need of adding the seismograms obtained for adjacent slowness panels. Some minor changes were made to

the code to avoid the need of recomputing the reflectivity coefficients after each run, by saving them to a temporary file.

Furthermore, some changes have been made to make it compatible with file formats and structural models in use in at the research laboratory of the Department of Earth Sciences of the University of Trieste and for easier comparison with the other method generating synthetic seismograms we use, the modal summation.

A.2.2 Strength and weakness of the method

The numerical integration over slowness is not performed over the entire axis at once. It is computed for panels of size limited by the memory usage of the program. It must be kept in mind that this is a numerical method, so the integration is not performed analytically and that therefore we have to choose the correct parameters for integration, that is the number of slownesses for every panel and the limits of the panel. Other methods, such as the modal summation, let us work with an analytical solution of the problem. This analytical solution, however, has enough accuracy (three significant digits) only in the case of $kr >= 10$ [Panza et al., 1973], that, in case of a frequency of $1Hz$ and a phase velocity of around $3km/s$ means a distance of about $5km$. Moreover, due to the limited phase velocity range considered, $r > h$.

A.3 Comparison of the reflectivity and modal summation methods

A.3.1 Validation of the two methods

A series of tests have been carried out by comparing signals obtained with the modal summation and the reflectivity methods, to validate both methods and to better understand their differences. Obviously in these tests, the source model and the structural model along the source-receiver path were the same, so most of the difference are due only to the different techniques employed to compute the synthetics.

The first tests have been carried out to validate the two methods. At the beginning we have chosen the source-receiver distance to be $40km$ to have both methods in their full range of functionality.

As long as we are in a range with $kr > 10$, $r > h$ and we consider only S waves the seismograms obtained with the two methods are comparable. The main difference is in fact a better modeling of the P waves for the reflectivity, whereas the modal summation method is better at modeling surface waves and much better from a computational point of view. In fact the modal summation is able to model only waves with a phase velocity lower than S-wave velocity in the half space.

When it comes to real data, reflectivity looks much better to model local events, in the near source field, that are outside the validity range of modal summation. When it comes to larger distances, the advantage of an analytical

method comes out in terms of a much better computational performance and a better modeling of surface waves.

In the following pages we present different tests, comparing modal summation and reflectivity seismograms, for different structures and sources, to validate respectively the two methods.

A.3.2 Comparison with a finite difference method

To have a better validation of the implementation of the method, the seismograms have been compared also to these obtained by using a numerical integration method, a finite difference scheme [Aochi and Douglas, 2006]. Due to the limitation of the finite difference modelling (space grid 100m, time interval 0.005s) the source time function of the method is slightly different (see Figure A.3), so the full waveform comparison has some limits. We can however compare the arrival times, and make some considerations on the shape of the waveforms.

The results show simulations for the vertical component only performed at a distance of $40km$, with a source placed at a depth of $5km$. The source has a pure strike-slip mechanism, magnitude $M_W = 5.0$ and the receiver has been placed at an azimuth of 295°.

A.3.3 Differences for near source distances

When the source-receiver distance is comparable to the receiver depth, the waveforms start to look different. However the tests at a small distance make less sense, since if we start to compare the signals with real signals we can't

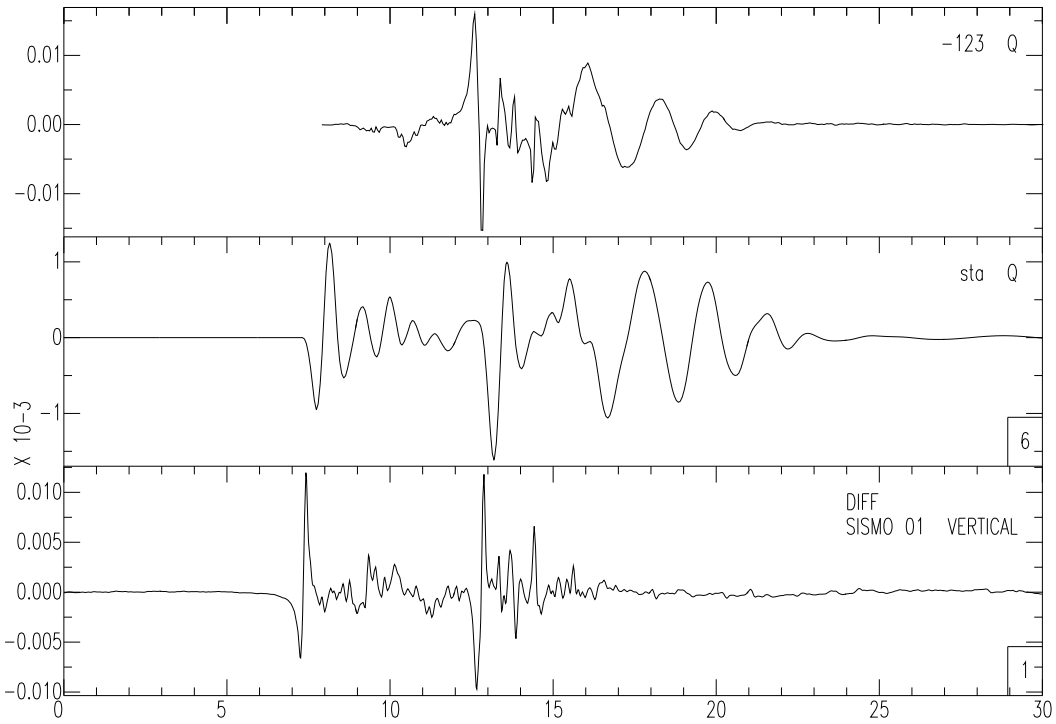

Figure A.1: Waveforms for a distance of 40 km with a strike slip source. From top to bottom: modal summation, numerical method and reflectivity

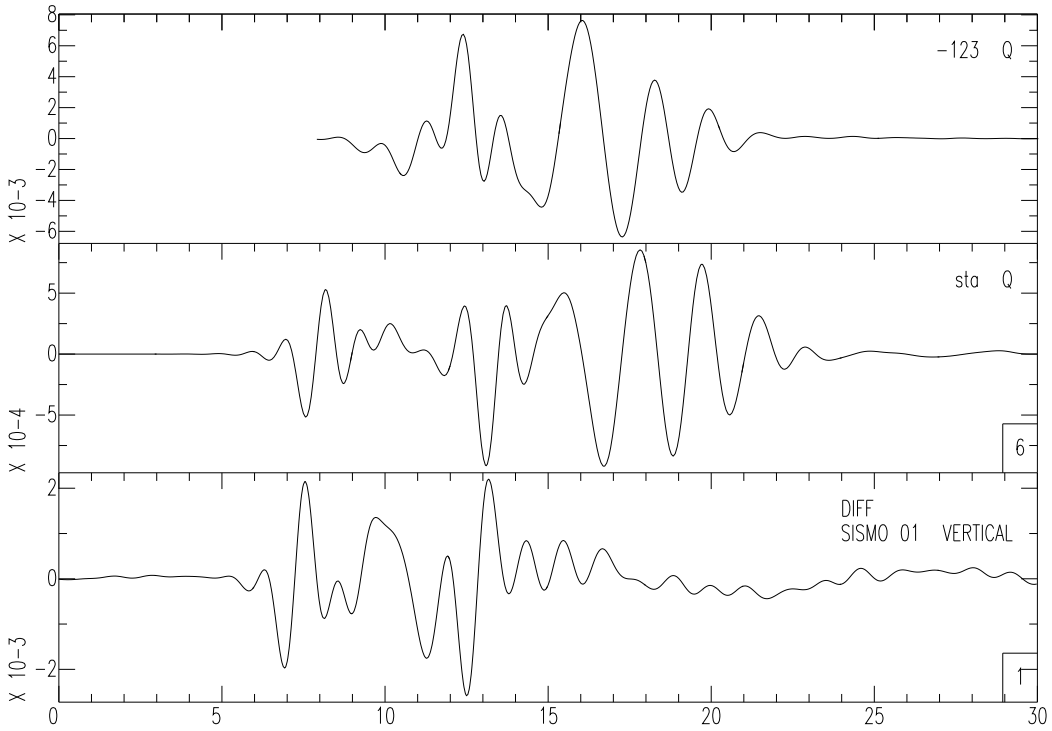

Figure A.2: Waveforms for a distance of 40 km with a strike slip source. From top to bottom: modal summation, numerical method and reflectivity LOW PASS FILTERED 1 Hz

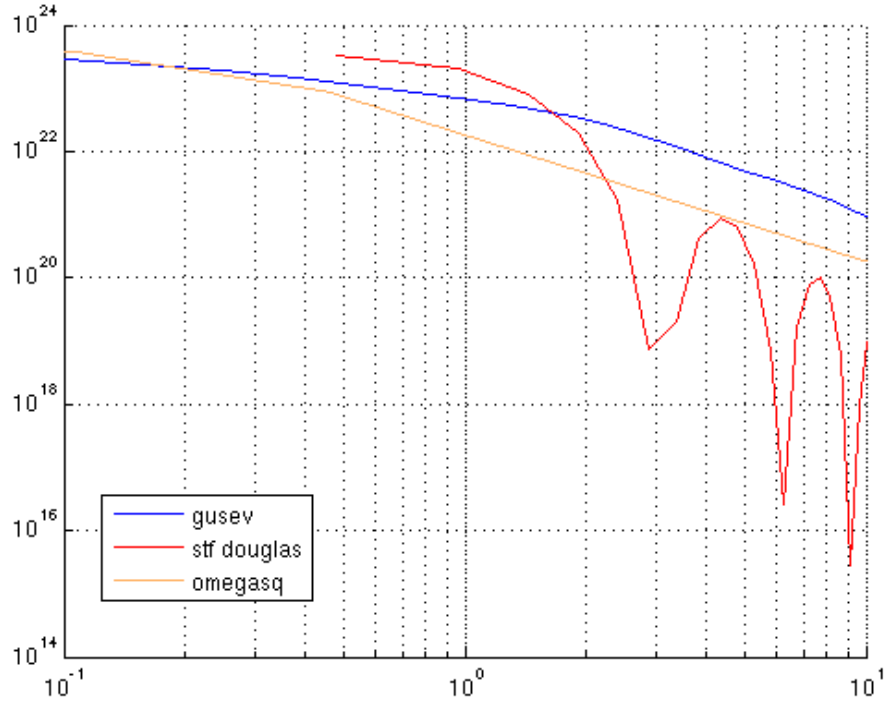

Figure A.3: Source time functions of the numerical method (Douglas) a B-spline function of order 4, the one used for for the other analytical methods (Gusev's curve) and another common source time function Ω^2 (omegasq)

neglect the fact that the seismic source is extended. We are presenting the tests, but this must be kept in mind and will be object of further development of the programs.

A.3.4 Far source distances

For distances much greater than the source depth we can notice that on one side the modal summation starts to better model also the arrival of the P waves, while on the other side the reflectivity starts to obtain smaller

amplitudes, due to a different attenuation model and a stronger numerical noise. While obtaining still reasonable seismograms, using the reflectivity method makes is unwise in this conditions, at least compared with the modal summation method.

A.4 Extended source modeling

A.4.1 The theory

To model an extended source to use it with the reflectivity method, we have used the same method used previously with the modal summation [Das et al., 1996] and [Saraò et al., 1998]. The main idea is to split the extended source in an array of point sources, and then summating the seismograms of every single element at a given receiver. The only thing to take into account is to have the spatial grid of the source smaller than the spatial resolution of the wavetrain.

Going into details, we can express the ground motion at the receiver u by

$$u_i(\mathbf{x},t) = \int_0^\infty dt' \int_\Sigma \int m_{jk}(\mathbf{x}',t') \cdot G_{ij,k}(\mathbf{x},t-t';\mathbf{x}',0) dS(\mathbf{x}') \qquad \text{(A.13)}$$

where $G_{ij,k}$ are the terms of the elastodynamic Green function tensor. If we assume that the faulting surface is a plane and that the faulting mechanism is constant all over the faulting surface, we can write Equation A.13 as

$$u_i(\mathbf{x},t) = \int_0^\infty dt' \int_\Sigma \int s(\mathbf{x}',t') \cdot g_i^{(\phi,\delta,\lambda)}(\mathbf{x},t-t';\mathbf{x}',0) dS(\mathbf{x}') \qquad \text{(A.14)}$$

$g_i^{(\phi,\delta,\lambda)}$ is the component of the response function the receiver site for a double couple source of given mechanism in the position $\mathbf{x}'$. Discretizing the source

we can write

$$\mathbf{u}(t) = \sum_{n=1}^{N} s_n(t) * \mathbf{g}_n(t) \tag{A.15}$$

where n is the cell index, N is the number of source cells due to discretization, and $*$ is the operator of convolution, while $s_n(t)$ is the source time function of every single cell.

This function can be splitted in a term due to rupture propagation on the fault plane ($\delta(t - \tau_n)$), and another that is the source time function of the element of source ($a_n(t)$). In this way we can obtain the final expression of ground motion for a complex source:

$$\mathbf{u}(t) = \sum_{n=1}^{N} a_n(t) * \delta(t - \tau_n) * \mathbf{g}_n(t) \tag{A.16}$$

$\mathbf{g}_n(t)$ are the Green functions that can be computed with different methods. In this study we will be using both the modal summation as a reference, and the reflectivity method.

Having to deal with a convolution, the best way to perform all the computation is to work in the frequency domain, to reduce convolutions to simple products.

In fact, in its implementation the algorithm has been splitted in three programs. The first to compute Green functions in the frequency domain, the second to define rupture times and the third to compute the summation over the source elements and to perform the inverse transform. Only the computation of Green functions is performed in a different way, once with the modal summation and once with the reflectivity.

Much care has been taken into obtaining Green functions with the same

temporal resolution of the modal summation, to make the two methods easily interchangeable.

A.4.2 Input files for the software

We present, as a reference of the parameters that can be used in the model, two sample input files for the software package developed.

The input file for the computation of Green Functions

```
================================================================================
|                  INPUT  PARAMETERS   FOR   SYEXT
================================================================================
 *STRUCUTRE FILENAME (asc)        : /home/delise/str/friul7w.str
aRAYLEIGH DISP. FUNC.(*.spr)      : /home/delise/str/friul7w.spr
 LOVE DISP. FUNC.    (*.spl)      : /home/delise/str/friul7w.spl
 HORIZONTAL COMPONENTS+           : 1 (0=none, 1=WE&NS, 2=plane paral.&perp.)
 HORIZ.G.F.(WE or Pl.paral.) ++(2): WEb.bin
 HORIZ.G.F.(NS or Pl.perpend.)    : NSb.bin
 VERTICAL G.F. (Z)           ++(2): Zb.bin
 Rayleigh eigenfunctions filename : eigenray.bin
 Love eigenfunctions filename     : eigenlov.bin
 Parameters filename              : par_fkob
 Check file                       : syext.chk
 Double precision output flag     : 0   (0=no, 1=yes)
 Rayleigh parameters file         : ray.param
 Love parameters file             : lov.param
 ------------------------------------------------------------------------
NUMBER OF STATIONS +++:   8
- - - - - - - - - - - - - - - - - - - - - - - - - - - - - - - - - - - - -  -
 STATIONS COORDINATES  ( LONGITUDE, LATITUDE      DEPTH (km))
 MOGG                 :  13 11 23   46 24 20
 CESC                 :  13 03 30   46 21 23
 VINO                 :  13 16 53   46 15 23
 30                   :  13 21 00   46 13 00
 MASA                 :  13 25 56   46 10 37
 40                   :  13 31 00   46 07 00
 50                   :  13 37 00   46 04 00
 DST                  :  13 48 09   45 39 35
                                        |<-50->|
================================================================================
 Ray. buried receivers file       : ray.depth
 Lov. buried receivers file       : lov.depth
================================================================================
 + NOTE: choose the components of the horizontal motion: NS/EW or plane paral./perp.
```

```
--------------------------------------------------------------------------------
++ NOTE: put into brackets where green func. filenames are defined:
   1 - output in ASCII form; 2 - output in BIN form; 0 - no output.
   If dealing with large number of cells it is suggested to save space using
   output in UNFORMATTED (BIN) form.
-----------------------------------------------------------------------
+++NOTE: The max number of receivers is defined in the file 'param.inc'
         with the statement : parameter (MAXREC=...)
=======================================================================

 NUMBER OF FAULTS     :   1        ( MAX 5 )

=======================================================================

  F I R S T   F A U L T

 REFERENCE POSITION   :  13 06 00   46 25 30  ( LONGITUDE, LATITUDE )

 FAULT ORIGIN RESPECT TO REFERENCE POSITION
 DIRECTION            :  00.00     ( DEGREES,  0/360 )
 RADIAL DISTANCE      :  00.00     ( KM,  +/- )
 TRANSVERSAL DISTANCE :   0.00     ( KM,  +/- )
 DEPTH                :  10.00     ( KM,  + ONLY )

 FAULT DESCRIPTION
 POINTS PER ROW       :  20        ( MAX 500 )         ! ALONG STRIKE !
 POINTS PER COLUMN    :  20        ( MAX 250 )          ! ALONG DIP !
 X-STEP               :   0.05     ( KM,  +/- )
 TYZ-STEP             :   0.05     ( KM,  + ONLY )
 TYZ-DEFINITION       :   1        ( 1, 2, 3 )  !ALONG 1=DIP 2=HOR 3=VERT!
 STARTING DEPTH       :  12.00     ( KM,  + ONLY )
 DIP                  :  22.00     ( DEGREES,  +90/-90 )
 STRIKE               : 328.00     ( DEGREES,  0/360 )
 RAKE                 : 186.00     ( DEGREES,  0/360 )
 ======================================================================
 FAULT RUPTURE

 NUCLEATION POINT     :             0       ( 0 YES,  N RUPT. FROM N-TH FAULT )
 NUCL. PT. COL. & ROW :      1      1
 TIME SHIFT           :          0.00       ( SECONDS )
 RUPTURE VELOCITY     :         72.00    S  ( PERC. OF S/P-WAVE VELOCITY; S, P )
 ======================================================================
 INPUT EIGENFUNCTIONS :      0              (COMPUTED=0, READ IN=1)
 INTERPOLATION        :      0              (NO=0, YES=1)
 **********************************************************************
```

The input file for the summation over the discrete source

```
 I N P U T   F I L E   F O R   FKOBNEW
=======================================================================
```

```
12345678901234567890123456789012345678901234567890123456789012345678901234567890
--------------------------------------------------------------------------------
NUMBER OF FAULTS:  1                    (MAX 5 FAULTS)
--------------------------------------------------------------------------------
check file                             : fkob.chk
NS P.PARALLEL seismograms              : smooth/NS
WE P.PERPENDICULAR seismograms         : smooth/WE
Z seismograms                          : smooth/Z
type of time series                ****: 2
--------------------------------------------------------------------------------
(****NOTE: 0 - displacement 1- velocity 2- acceleration)
~~~~~~~~~~~~~~~~~~~~~~~~~~~~~~~~~~~~~~~~~~~~~~~~~~~~~~~~~~~~~~~~~~~~~~~~~~~~~~~~
format of output seismograms           : 0  (0-sac, 1-xy, 2-y )
~~~~~~~~~~~~~~~~~~~~~~~~~~~~~~~~~~~~~~~~~~~~~~~~~~~~~~~~~~~~~~~~~~~~~~~~~~~~~~~~

   F I R S T   F A U L T

file used to compute 'green functions': syext03.inp
file with rupturing times              : ruptimes.out
file with moment distribution      (1): 1.mom
file with rise times               (0): 0
NS or P.PARALLEL green functions  *(2): NSb.bin
WE P.PERPENDICULAR green functions*(2): WEb.bin
Z green functions                 *(2): Zb.bin
- - - - - - - - - - - - - - - - - - - - - - - - - - - - - - - - - - - - - - - -
*NOTE: 0-skip  1-ASCII 2-BIN
~~~~~~~~~~~~~~~~~~~~~~~~~~~~~~~~~~~~~~~~~~~~~~~~~~~~~~~~~~~~~~~~~~~~~~~~~~~~~~~~
total seismic moment (all faults)   **: 1.50000e+03 (*10^20 dyne cm)
moment smoothing at borders        ***: 0.00000e+00
- - - - - - - - - - - - - - - - - - - - - - - - - - - - - - - - - - - - - - - -
** ignored if file with non-uniform moment distribution is given
***NOTE : 0.0- no smoothing  1.0- smoothed till the centre of the fault
~~~~~~~~~~~~~~~~~~~~~~~~~~~~~~~~~~~~~~~~~~~~~~~~~~~~~~~~~~~~~~~~~~~~~~~~~~~~~~~~

   S E C O N D   F A U L T

file used to compute 'green functions': fg2.inp
file with rupturing times              : fg2.out
file with moment distribution      (0): 0
file with rise times               (0): 0
NS or P.PARALLEL green functions  *(2): NS2.bin
WE P.PERPENDICULAR green functions*(2): WE2.bin
Z green functions                 *(2): Z2.bin
- - - - - - - - - - - - - - - - - - - - - - - - - - - - - - - - - - - - - - - -
*NOTE: 0-skip  1-ASCII 2-BIN
~~~~~~~~~~~~~~~~~~~~~~~~~~~~~~~~~~~~~~~~~~~~~~~~~~~~~~~~~~~~~~~~~~~~~~~~~~~~~~~~
total seismic moment (all faults)   **: 1.10000e+04 (*10^20 dyne cm)
moment smoothing at borders        ***: 0.20000e-00
- - - - - - - - - - - - - - - - - - - - - - - - - - - - - - - - - - - - - - - -
** ignored if file with non-uniform moment distribution is given
***NOTE : 0.0- no smoothing  1.0- smoothed till the centre of the fault
```

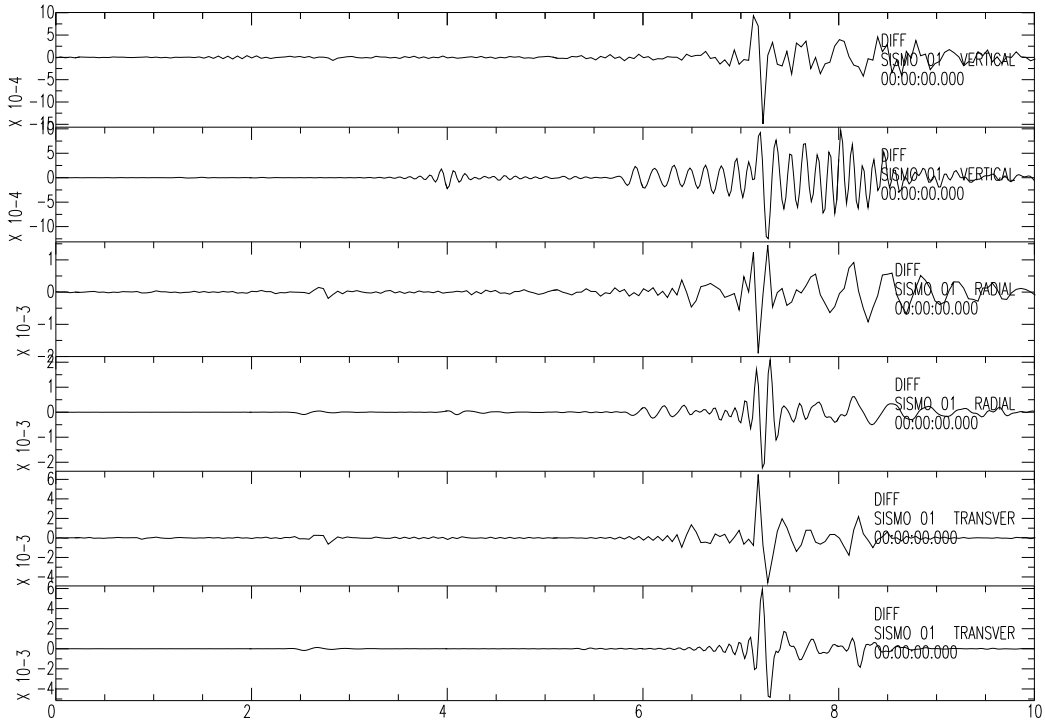

Figure A.4: Modal summation (upper traces) and reflectivity (lower traces) signals for a point source event at a distance of 21 km, a source depth of 7.6 km and a strike, dip and rake respectively of 15, 13 and 75 degrees.

~~~~~~

A.4.3 Comparison with real data

With an extended source, it makes much more sense to compare the signals recorded at near-source events with real recordings of events, possibly at different source-receiver distances.

To test the extended source synthetic seismograms we have chosen the event of February 14,2002, located in the area near Moggio Udinese (UD), almost at the geographical center of the network managed by our department
~~~~~~

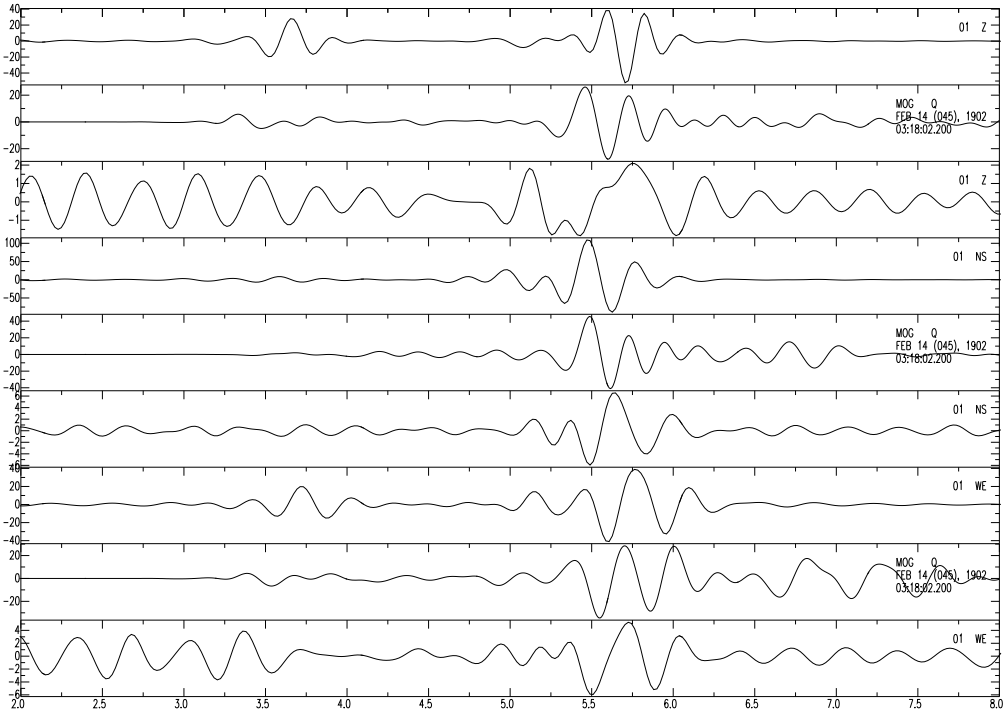

Figure A.5: From top to bottom: reflectivity seismograms, real data and modal summation seismograms for Z, N and E components, LP 5Hz for the MOGG station

and just below the stationa MOGG and CESC, located less than $10km$ from the epicenter. For more information on the event in itself, and on the source parameters and models used in the modelling please see Chapter 2.4.

The reflectivity method natively models the data in displacements, so they have to be differentiated to be comparable to the acceleration by multiplying the signals by $-i\omega$ in the frequency domain.

In a such limit situation for the modal summation, we can see in figure A.5 the differences between the two methods, always compared with real data. The modal summation waveforms modelled show unrealistic amplitudes and

unmodelled arrivals, while the reflectivity method shows a decent agreement with the data. It must be kept in mind, however, that we are beyond the limits of validity of the modal summation method and that this limit has been the main reason to study the reflectivity method.

Appendix B

Localization algorithms

B.1 Event location

One basic study of a seismic event consists in defining as accurately as possible its location. This is crucial for all further studies, and critical for civil defense activities to define the area affected by the event.

B.1.1 Single-event location algorithms

The problem of the location of earthquakes from seismic data is one of the first inverse problems in geophysics. Since 132 AD, when the fist seismoscope was created in China by Zhang Heng, whose purpose was to detect propagation direction of waves, many location methods have been proposed.

One station location

Even when having only one three-component station it is still possible to locate an earthquake, albeit with big uncertainties. From the time difference between the P and S arrivals it is possible to obtain a rough estimate of the distance of the epicenter from the station, while from the amplitude ratio of the horizontal components it is possible to determine the direction of propagation of the incoming wavetrain.

Location with more stations

With at least 3 stations it is possible to locate an earthquake with a much easier and more stable method. From the difference between P and S waves of each station it is possible to estimate the distance of the epicenter from the station. Three distances from three points define three circles, that intersect near a common point, the epicenter. With more than three station, it might be necessary a statistical approach (e. g. least squares) to estimate the best location and the related errors.

Geiger's method

Having more data available, it is obvious that one has to use a more sophisticated method. Having more station data, even if we discard the ratios of the horizontal component, leads us into an overdetermined problem, since the variable vector for which we are solving the problem contains only the 3 coordinates and the origin time [Geiger, 1910].

To locate the epicentre of an earthquake the travel-time difference be-

tween the shear (S) and compressional (P) waves is used to estimate the distance from a seismological observatory to the earthquake source. Due to his observational work, while producing the seismic bulletin at Göttingen, Geiger had realized that the determination of the S-arrivals is difficult, erroneous, and sometimes even impossible. Therefore, he searched for another possibility to locate earthquakes with accurate P-arrival times only. The Geiger method (1910) is formulated as an inverse problem. Starting from a guessed epicentre and origin time a systematic solution is found, using a linearization procedure(first order Taylor series) and a least-squares inversion. The depth of the earthquakes is implicitly assumed to be zero or a fixed crustal depth, because the occurrence of deep hypocentres was not considered at that time.

Grid search method

Another common location method is the so called "grid search" method. This method consists in a non linear inversion of travel times.

Travel times are pre computed on a grid of possible solutions once and then stored. To locate an event arrival times recorded are compared to those predicted for the full grid of possible epicenters.

To optimize this method, like for any non linear inversion, many algorithms can come in help in avoiding exploring the full parameter space. However, for modern computing resources, even the full exploration of the parameter space, provided the grid in reasonably sparse, is a quick task. This explains why this method is frequently used in fully automatic location

programs, such as those used in real time systems.

To use it in real time, provided it is used only a 1D velocity model, travel times can be computed once and then stored, for faster location.

B.1.2 Multiple-event location algorithm

A strong earthquake is usually followed by many smaller events, located near the main shock in space and in time. The small distance can be useful to obtain better relative locations of such events, since the epicenter-station path is assumed to be similar for each station.

We can expose the problem considering every i^{th} station and j^{th} earthquake, with a source vector $\mathbf{m}_j(x_j, y_j, z_j, t_j)$ that contains the hypocentral coordinates and the origin time. For every station, we can consider the theoretical arrival time $t_j^i = t_j^i(\mathbf{m}_j, \mathbf{v}_j^i)$ with $\mathbf{v}_j^i$ the velocity along the path connecting epicenter j with station i. Our aim will be to minimize the travel time misfit for every station, that is

$$\Delta_j^i =^{obs} t_j^i -^{pred} t_j^i = \int_l \mathbf{\Delta}\rho_j^i dl + \frac{\partial t_j^i}{\partial \mathbf{m}} \cdot \mathbf{\Delta m}_j + h.o.t. \tag{B.1}$$

where dl is the ray segment in the reference model and $\mathbf{\Delta}\rho$ is the perturbation in slowness. The first approach to the solution of the problem is the linearization of the problem, that is writing.

$$\Delta_j^i = \Delta s_j^i + \frac{\partial t}{\partial \mathbf{m}} \cdot \Delta \mathbf{m}_i \tag{B.2}$$

The travel time anomalies can be divided in three terms: source mislocation, travel time anomalies and the ones due to the linearization. This is

clearer if we express the solution in matrix form:

$$\mathbf{G}_j \cdot \mathbf{\Delta m}_j + \mathbf{S}_j \cdot \mathbf{\Delta s}_j = \mathbf{\Delta d}_j \tag{B.3}$$

where $\mathbf{G}_j = \frac{\partial t_j^i}{\partial \mathbf{m}_j}$, $\Delta \mathbf{m}_j$ is the perturbation of $\mathbf{m}$, $\mathbf{S}_j$ is the partial derivative of the path with respect to every station, $\mathbf{\Delta s}_j$ the path anomaly vector and $\mathbf{\Delta d}_j$ the residual vector.

This representation can be extended to consider multiple events. In this case we can express it as

$$\mathbf{G} \cdot \mathbf{\Delta m} + \mathbf{S} \cdot \overline{\mathbf{\Delta s}} + \delta\varsigma = \mathbf{\Delta d} \tag{B.4}$$

where $\delta\varsigma$ is due to the differences in path anomalies between the events.

Having to deal with multiple events there are two kinds of simplification we can perform. The first is to consider the average path anomaly for all the events, taking $\delta\varsigma = 0$, thus ending in the situation of a so called "Tight Cluster" of events.

Going further, we can assume that also $\mathbf{G}$ remains constant for all the events, reducing the computational load of the partial derivatives. This approximation is the so called "Very Tight Cluster" of earthquakes.

Joint Hypocenter Determination

The Joint Hypcenter Determination [Douglas, 1967] like many of these methods, is based on the principle that station correction for regional events could be assumed equal. The relocation is in fact, at least for the so called "master events", an inversion for both the location and the station correction.

Smaller events are later located with the station corrections obtained from the inversion.

So we can say that JHD performs a simultaneous inversion of $\mathbf{\Delta m}$ and $\delta\varsigma$. This is performed by applying the projector $\mathbf{Q}_S = \mathbf{I} - \mathbf{S}\mathbf{S}^\dagger$ to Equation B.4 to determine $\mathbf{\Delta m}$ and $\mathbf{Q}_G = \mathbf{I} - \mathbf{G}\mathbf{G}^\dagger$ to determine $\delta\varsigma$.

Hypocentral Decomposition (HDC)

The hypocentral decomposition consists, as its name states, in a decomposition of the central location of the cluster of earthquakes and following location of relative cluster vectors.

HDC is very similar to JHD, with the difference that HDC applies only if all partial derivatives of travel times for a cluster are not significantly different, that is the radius of diffusion of events is very small compared to the station-receiver distance.

In mathematical terms, this means that we apply the projector $\mathbf{Q}_S = \mathbf{I} - \mathbf{S}\mathbf{S}^\dagger$ to EquationB.4, leaving only the terms with the unknown $\delta\mathbf{m}$. It must be kept in mind that the centroid vector $\Delta\mathbf{m}$ is strongly correlated with the station velocity corrections $\overline{\Delta\mathbf{s}}$.

Double Difference

The double difference method is based on the principle of using for the location, rather than travel times, differential travel times computed relatively one reference event.

This means applying to Equation B.4 is the so called “double difference

operator"

$$\mathbf{Q}_{DD} = \begin{pmatrix} 1 & -1 & . & . & . \\ 1 & . & -1 & . & . \\ . & . & . & . & . \\ . & . & . & . & -1 \\ 1 & . & . & 1 & 1 \end{pmatrix} \tag{B.5}$$

Applying it to the path anomalies $\mathbf{S} \cdot \overline{\mathbf{\Delta s}}$ makes them vanish. This implies we do not get from DD the station path corrections, obtaining only relative locations.

B.1.3 Location methods implying reanalysis of picks

The procedure of locating earthquakes has various sources of error: multiple-event algorithms let us take into account errors due to the Earth model. Modern location algorithms let us overcome another source of error, the human factor. All the previously presented methods are based on the availability of arrival times that need to be picked by an operator on the seismograms.

These methods require a complete reanalysis of waveforms, a much more complex problem than the simple analysis of arrival times. In exchange, they can refine or even detect automatically arrival times.

In this case, rather than analyzing P and S waves arrival times, usually it it used Lg. To identify the relative difference between the arrival times the algorithms use waveform cross correlation. To compute differential arrival time we search for the maximum cross-correlation between the waveforms of

an aftershock and the one of the main event.

Once obtained the differential arrival times, it is then possible to apply one of the previously presented methods.

B.1.4 The network used in this study

This study is mainly based on data related to the 2004 Bovec earthquake sequence, recorded by a large set of stations. The permanent stations in the area belong to many research institutions: the *Agencija Republike Slovenije za okolje, urad za seizmologijo* (ARSO) mantains the network on the Slovenian territory, the *Zentralanstalt fr Meteorologie und Geodynamik* (ZAMG) mantains the Austrian Network, while on the Italian territory we can find the networks of the *Istituto Nazionale di Oceanografia e Geofisica Sperimentale* (INOGS) and of the *Dipartimento di Scienze della Terra - Università di Trieste* (DST). After the main shock, a temporary network has been deployed, mainly by ARSO, INOGS (in collaboration with the *Istituto Nazionale di Geofisica e Vulcanologia* -INGV), DST (in collaboration with *Servizio Sismico Nazionale*-SSN)

The network consist of various kinds of stations: short-period ones, strong-motion ones and broad-band ones. All had absolute timing, supplied by DCF or GPS. The maximum sampling frequencies, which give us the time resolution of the recordings, are set for all station above $100Hz$

B.1.5 JHD and local events

All the methods described above were developed for teleseismic events. A reasonable question is if it makes sense using them with such a local network, positioned in close proximity of the events.

When working with local earthquake sequences, most algorithms can give good results in terms of the relative location. The problem has been to obtain a good absolute location. DD and HDC are rather inappropriate for the usage, since DD by definitions gives only relative locations, while HDC with its strong tradeoff between station corrections and absolute locations is in a similar situation.

Adding the station corrections to JHD should be the most conservative solution, at least compared to routine location algorithm.

Appendix C

Source mechanism waveform inversion

C.1 Source parameter inversion

C.1.1 The problem

Apart from location, another task we encounter when we study an earthquake is the determination of its source parameters. The source mechanism is completely described by the full moment tensor of the source. In the area we are studying, however, the earthquakes are due to tectonic stresses, and isotropic and CLVD components are not to be expected, such as in a volcanic area. A reasonable simplification is therefore to consider the source mechanism simply as an oriented double couple.

If to locate an earthquake most algorithms need only the picking of wave arrival times, for the source mechanism determination we need at least well

distributed wave polarities, but better the full waveform data. We need also a direct waveform modelling algorithm, a trial source model (in some cases) and a velocity model.

C.1.2 The approach used

Based on the assumptions made in previous section, we follow a linearized waveform inversion approach [Mao et al., 1994]. This algorithm has been recently refined by the addition of partial derivatives with respect to source parameters for Love waves [Delise, 2003].

The generalized direct problem is

$$\mathbf{d} = \mathbf{G}\mathbf{m} \tag{C.1}$$

where $\mathbf{d}$ is a vector in the data space, $\mathbf{m}$ is a vector in the parameter space, and $\mathbf{G}$ is a matrix that represents our model.

From algebra we know that for a rectangular matrix like $\mathbf{G}$ we can't have an unique inverse, but a particular solution can be given by

$$\mathbf{m_p} = \mathbf{G_p^{-1}}\mathbf{d} \tag{C.2}$$

A linearized approach means that we start with a trial solution. We can express every seismogram as a first-order truncated Taylor polynomial, containing the partial derivatives with respect to all the parameters we need to know.

$$s(p_1,\ldots,p_m,t) = s(p_{10},\ldots,p_{m0}) + \frac{\partial}{\partial p_1}s(p_{10},\ldots,p_{m0})\Delta p_1 + \ldots \\ \ldots + \frac{\partial}{\partial p_m}s(p_{10},\ldots,p_{m0})\Delta p_m \quad \text{(C.3)}$$

where s is the seismogram, p a parameter, t the time and m the number of parameters. Parameters with index $_0$ are related to the trial solution. Using Equation C.3 we can replace in Equation C.1 to the vector $\mathbf{d}$ the residuals of the data with respect to the trial solution $s(p_{10},\ldots,p_{m0})$ and to the matrix $\mathbf{G}$ a matrix of the partial derivatives $\mathbf{A}$ defined as follows.

$$\mathbf{A} = \begin{matrix} \frac{\partial s_1(t_1)}{\partial\theta} & \frac{\partial s_1(t_1)}{\partial\delta} & \frac{\partial s_1(t_1)}{\partial\lambda} & \frac{\partial s_1(t_1)}{\partial h} & \frac{\partial s_1(t_1)}{\partial x} & \frac{\partial s_1(t_1)}{\partial y} & \frac{\partial s_1(t_1)}{\partial w_1} & \cdots & \frac{\partial s_1(t_1)}{\partial w_k} \\ \vdots & \vdots & \vdots & \vdots & \vdots & \vdots & \vdots & \cdots & \vdots \\ \frac{\partial s_1(t_{m1})}{\partial\theta} & \frac{\partial s_1(t_{m1})}{\partial\delta} & \frac{\partial s_1(t_{m1})}{\partial\lambda} & \frac{\partial s_1(t_{m1})}{\partial h} & \frac{\partial s_1(t_{m1})}{\partial x} & \frac{\partial s_1(t_{m1})}{\partial y} & \frac{\partial s_1(t_{m1})}{\partial w_1} & \cdots & \frac{\partial s_1(t_{m1})}{\partial w_k} \\ \cdots & \cdots & \cdots & \cdots & \cdots & \cdots & \cdots & \cdots & \cdots \\ \frac{\partial s_n(t_1)}{\partial\theta} & \frac{\partial s_n(t_1)}{\partial\delta} & \frac{\partial s_n(t_1)}{\partial\lambda} & \frac{\partial s_n(t_1)}{\partial h} & \frac{\partial s_n(t_1)}{\partial x} & \frac{\partial s_n(t_1)}{\partial y} & \frac{\partial s_n(t_1)}{\partial w_1} & \cdots & \frac{\partial s_n(t_1)}{\partial w_k} \\ \frac{\partial s_n(t_{mn})}{\partial\theta} & \frac{\partial s_n(t_{mn})}{\partial\delta} & \frac{\partial s_n(t_{mn})}{\partial\lambda} & \frac{\partial s_n(t_{mn})}{\partial h} & \frac{\partial s_n(t_{mn})}{\partial x} & \frac{\partial s_n(t_{mn})}{\partial y} & \frac{\partial s_n(t_{mn})}{\partial w_1} & \cdots & \frac{\partial s_n(t_{mn})}{\partial w_k} \end{matrix} \quad \text{(C.4)}$$

The matrix we will have to invert in this case is $\mathbf{A}$ rather than $\mathbf{G}$. The inversion of the matrix has been performed with a Singular Values Decomposition method, with the addition of a damping parameter to avoid the effect of smaller eigenvalues.

The partial derivatives of the synthetic seismograms can be computed numerically or analytically. One of the main advantages of using the modal summation method for synthetic seismograms is the fact that it is possible to compute them analytically, resulting in a reduction of computation time.

C.1.3 Input data

Such an example, we show the input file for the inversion program, to give a full picture of the parameters necessary to run the inversion.

```
0  50   35.                                  Nb.Iter.More,Nb.Iter.1st,MaxDurPlot

0  0  4                                      FirstMode, LastMode, Interp.Factor
0.01 0.01 0.01                               Damping Ratios Syst. STF, MEC, LOC
9   0.2  0.1                                 Nb.Triang.,Tria.Width,Tria.Spacing
1. 1. 1. 1. 1. 1. 1. 1. 1.                   Initial triangle amplitudes
80.0 50.0 50.0  6.06  46.514 13.004          Init.Str,Dip,Rake,Dep,SouLat,SouLon
0                                            [FinitnessFlag,Vr/Vs,KmStrk,KmAnti]
 7 30 00                                     Event Origin time: hour min sec
2                                            Number of stations
LNOS  T        ............................. STATION name, Component(s)
46.66 13.0 0.                                Station LatN dg, LongE dg, Depth km
../str/friul7w.spl                           [Path Structure spectrum]
0 0 0                                        Instr.,GaussFilt.,VarFilt. options
1.                                           NoInst.: Mag.in Data_unit/m(/s)(/s)
0. 0. 0.                                     GauFil:[CutFr,PeakFr/CutFr,AmpACut]
                                             VarFil:[file with Velocity limits]
TNOSU01.sac                                  Data file name (sac)
NOSU  Z R      ............................. STATION name, Component(s)
46.66 13.0 0.                                Station LatN dg, LongE dg, Depth km
../str/friul7w.spr                           [Path Structure spectrum]
0 0 0                                        Instr.,GaussFilt.,VarFilt. options
1.                                           NoInst.: Mag.in Data_unit/m(/s)(/s)
0. 0. 0.                                     GauFil:[CutFr,PeakFr/CutFr,AmpACut]
                                             VarFil:[file with Velocity limits]
ZNOSU01.sac                                  Data file name (sac)
RNOSU01.sac
```

C.1.4 Error evaluation

The linearized approach has one drawback: the difficulty in applying a rigorous error theory to the events hence to have an estimate of the quality of the inversion. Various attempt have been carried out in the search for an estimate.

The first approach, rather empirical, has been to perform a gird search for a sample event. The results are shown in Figure C.1.

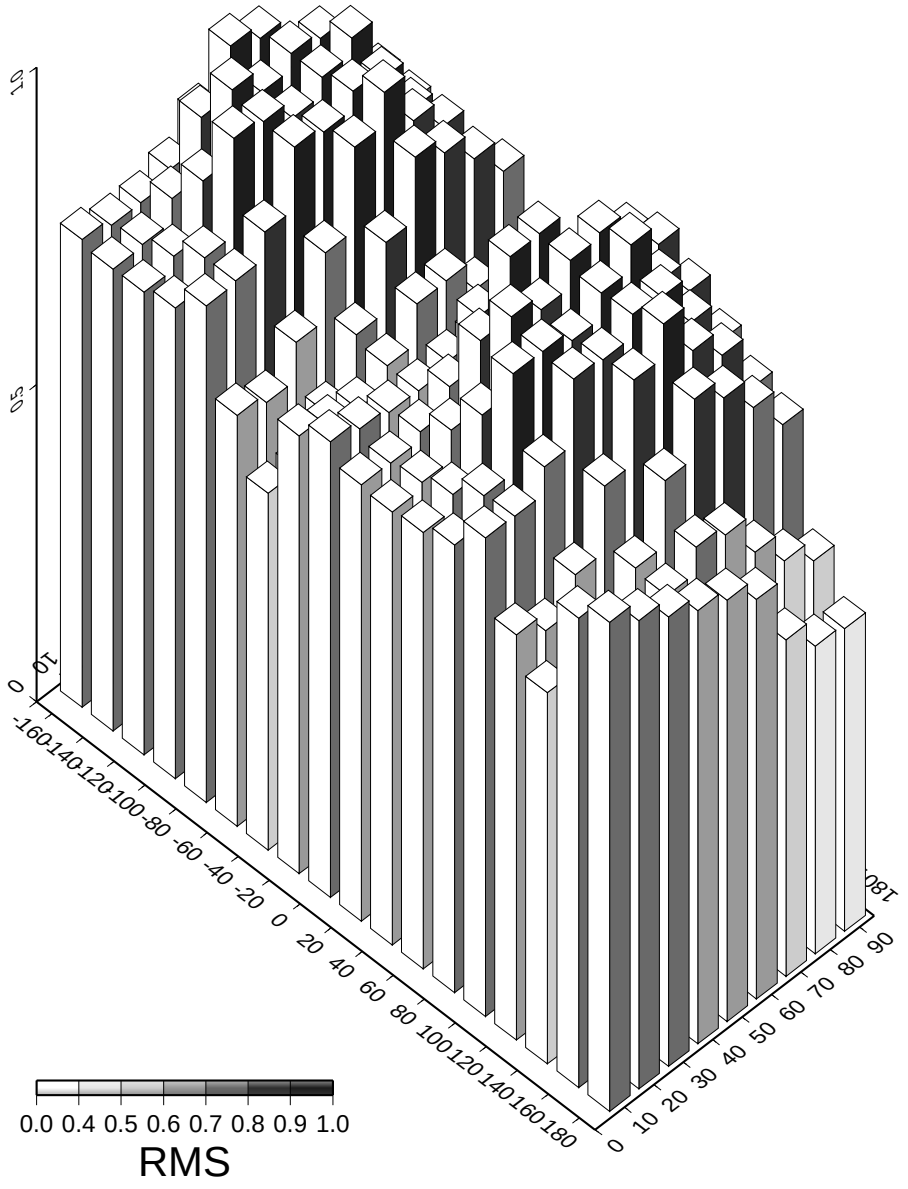

Figure C.1: Residuals for a grid search performed in the source mechanisms space

Another approach, less time consuming, has been to correlate the residuals of the inversion with the variation of the parameters. Then we chose an acceptable misfit on the residuals, 10%, and due to that we calculate the error on the parameters.

This approach is based on the assumption of a correlation between residuals and misfits. Since the full inversion is based on the linearization, this simplification can be acceptable, or at least should not introduce greater uncertainties. From Figure C.1 we can have an idea of how much error we are introducing with this approximation. Approaching the minimum, at least for the two parameters explored in the grid search, we can observe a decent degree of linearity, justifying then our approach.

For all the events taken into account the average error, taken with a 10% error on residuals is 8° for strike, 14° for dip and 19° for rake. The algorithm returns much bigger errors on rake rather than dip or rake, reasonably.

Bibliography

[Aki, 1965] Aki, K. (1965). Maximum likelihood estimate of b in the formula $\log N = a - bM$ and its confidence limits. *Bulletin Earthquake Res. Institute Tokyo Univ.*, 43:237–239.

[Anderson and Jackson, 1987] Anderson, H. and Jackson, J. (1987). Active tectonics of the adriatic region. *Geophysical journal of the Royal Astronomical Society*, 91(3):937–983.

[Aochi and Douglas, 2006] Aochi, H. and Douglas, J. (2006). Testing the validity of simulated strong ground motion from the dynamic rupture of a finite fault by using empirical equations. *Bulletin of Earthquake Engineering*, 4:211–229.

[Aoudia, 1998] Aoudia, A. (1998). *Active Faulting and Seismological Studies for Earthquake Hazard Assessment*. PhD thesis, University of Trieste.

[Aoudia et al., 2000] Aoudia, A., Saraó, A., Bukchin, B., and Suhadolc, P. (2000). The 1976 Friuli (NE Italy) Thrust Faulting Earthquake: A Reappraisal 23 Years Later. *Geophysical Research Letters*, 27:573–999.

[Bada et al., 2001] Bada, G., Horváth, F., Cloeting, S., Coblentz, D. D., and Tóth, T. (2001). Role of topography induced gravitational stresses in basin inversion: The case study of the Pannonian basin. *Tectonics*, 20:343–363.

[Bajc et al., 2001] Bajc, J., Aoudia, A., Saraò, A., and Suhadolc, P. (2001). The 1998 Bovec-Krn mountain (Slovenia) earthquake sequence. *Geophysical Research Letters*, 28(9):1839–1842.

[Bragato et al., 2003] Bragato, P., Costa, G., Horn, N., Michelini, A., Mocnik, G., and Živčić, M. (2003). Real-Time Data and Network Integration in the southern Alps. *EGS - AGU - EUG Joint Assembly, Abstracts from the meeting held in Nice, France, 6 - 11 April 2003, abstract #8690*, pages 8690–+.

[Bressan et al., 2003] Bressan, G., L., B. P., and Venturini, C. (2003). Stress and Strain Tensors Based on Focal Mechanisms in the Seismotectonic Framework of the Friuli-Venezia Giulia Region (Northeastern Italy). *Bull. Seism. Soc. Am.*, 93:1280–1297.

[Bressan et al., 1998] Bressan, G., Snidarcig, A., and Venturini, C. (1998). Present state of tectonic stress of the Friuli area (eastern Southern Alps). *Tectonophysics*, 292:211–227.

[Carulli et al., 1990] Carulli, G. B., Nicolich, R., Rebez, A., and Slejko, D. (1990). Seismotectonics of the Northwest external Dinarides. *Tectonophysics*, 179(1-2):11–25.

[Channel and Horvath, 1976] Channel, J. E. and Horvath, F. (1976). The African Adriatic promontory as a paleografic premise for Alpine Orogeny and Plate Movements in the Carpatho-Balkan region. *Tectonophysics*, 35:71–101.

[Costa et al., 1993] Costa, G., Panza, G. F., Suhadolc, P., and Vaccari, F. (1993). Zoning of the Italian Territory in Term of Expected Peak Ground Acceleration Derived from Complete Synthetic Seismograms. *J. Appl. Geophys.*, 30:149–160.

[Costa et al., 2006] Costa, G., Suhadolc, P., Delise, A., Moratto, L., Furlanetto, E., and Fitzko, F. (2006). Estimation of site effects at some stations of the Friuli (NE Italy) accelerometric network (RAF). *3rd International Symposium on "The effects of Surface Geology on Seismic Motion" ESG 2006- Grenoble.*

[Das et al., 1996] Das, S., Suhadolc, P., and Kostrov, B. V. (1996). Realistic inversions to obtain gross properties of the earthquake faulting process. In: C.-I. Trifu (ed.), Seismic Source Parameters: from Microearthquakes to Large Events. *Tectonophysics*, 261:165–177.

[Delise, 2003] Delise, A. (2003). Inversione linearizzata di forme d'onda sismiche per parametri di sorgente: estensione alle onde di Love ed applicazione agli eventi del monte Nevoso (Snežnik) - Slovenia. Thesis, Dip. di Scienze della Terra, University of Trieste.

[Douglas, 1967] Douglas, A. (1967). Joint epicentre determination. *Nature*, 215:47–48.

[ETHZ, 2006] ETHZ (2006). Moment tensors database. http://www.seismo.ethz.ch/.

[Fitzko et al., 2007] Fitzko, F., Costa, G., Delise, A., and Suhadolc, P. (2007). Site Effects Analyses in the old city centre of Trieste (NE Italy) using accelerometric data. *Journal of Earthquake Engineering*, 11:56–71.

[Fitzko et al., 2005] Fitzko, F., Suhadolc, P., Aoudia, A., and Panza, G. F. (2005). Constraints on the location and mechanism of the 1511 Western Slovenia earthquake from active tectonics and modeling of macroseismic data. *Tectonophysics*, 404:77–90.

[Fuchs and Müller, 1971] Fuchs, K. and Müller, G. (1971). Computation of Synthetic Seismograms with the Reflectivity Method and Comparison with Observations. *Geophys. J. R. astr. Soc.*, 23:417–433.

[Geiger, 1910] Geiger, L. (1910). Herdbestimmung bei Erdbeben aus den Ankunftszeiten. *Nachrichten von der Königlichen Gesellschaft der Wissenschaften zu Göttingen, Mathematisch-Physikalische Klasse*, pages 331–349.

[Gilbert and Backus, 1966] Gilbert, F. and Backus, G. E. (1966). Propagator matrices in elastic wave and vibration problems. *Geophysics*, 31:326–332.

[Giorgetti, 1976] Giorgetti, F. (1976). Isoseismal map of the May, 6 1976 Friuli earthquake. *Boll. Geofis. Teor. Appl.*, 19:637–655.

[Herak et al., 1995] Herak, M., Herak, D., and Markušić, S. (1995). Fault-plane solutions for earthquakes (1956-1995) in Croatia and neighbouring regions. *Geofizika*, 12:43–56.

[INOGS, 2002] INOGS (1977-2002). Bollettino della rete sismometrica Del Friuli Venezia Giulia. Technical report, INOGS.

[Kennett, 1983] Kennett, B. L. N. (1983). *Seismic wave propagation in stratified media*. Cambridge university press.

[Kennett and Kerry, 1979] Kennett, B. L. N. and Kerry, N. J. (1979). Seismic waves in a stratified half space. *Geophys. J. R. astr. Soc.*, 57:557–583.

[King et al., 1994] King, G. C. P., Stein, R. S., and Lin, J. (1994). Static Stress Changes and the Triggering of Earthquakes. *Bull. Seismol. Soc. Am.*, 84:935–953.

[Lay and Wallace, 1995] Lay, T. and Wallace, T. C. (1995). *Modern global seismology*. Academic Press.

[Mao et al., 1994] Mao, W. J., Panza, G. F., and Suhadolc, P. (1994). Linearized waveform inversion of local and near regional events for source mechanism and rupturing processes. *Geophys. J. Int*, 116:784–798.

[Marrara et al., 2001] Marrara, F., Saraò, A., and Suhadolc, P. (2001). Amplifications of the seismic ground motion in Gemona (NE-Italy) due to the 1998 Bovec-Krn earthquake. *Boll. Geofis. Teor. Appl.*, 42(3-4):209–217.

[Mednet, 2006] Mednet (2006). Moment tensors database. http://mednet.ingv.it/.

[Okada, 1992] Okada, Y. (1992). Internal Deformation due to shear and tensile faults in a half-space. *Bull. Seism. Soc. Am.*, 82(2):1018–1040.

[Panza et al., 1973] Panza, G. F., Schwab, F. A., and Knopoff, L. (1973). Multimode Surface Waves for Selected Focal Mechanisms I. Dip-Slip Sources on a Vertical Fault Plane. *Geophys. J. R. astr. Soc.*, 34:265–278.

[Perniola et al., 2003] Perniola, B., Bressan, G., and Pondrelli, S. (2003). Changes in failure stress and stress transfer during the 1976-1977 Friuli earthquake sequence. *Geophys. J. Int.*, 156:297–306.

[Platt et al., 1989] Platt, J. P., Behrmann, J. H., Cunningham, P. C., Dewey, J. F., Helman, M., Parish, M., Shepley, M. G., Wallis, S., and Weston, P. J. (1989). Kinematics of the Alpine arc and the motion history of Adria. *Nature*, 337:158–161.

[Poljak et al., 2000] Poljak, M., Živčić, M., and Zupančič, P. (2000). The Seismotectonic Characteristics of Slovenia. *Pure Appl. Geophys.*, 157:37–55.

[Saraò et al., 1998] Saraò, A., Das, S., and Suhadolc, P. (1998). Effect of non uniform station coverage on the inversion for earthquake rupture history for a Haskell-type source model. *Journal of Seismology*, 2:1–25.

[Scholz, 2002] Scholz, C. H. (2002). *The Mechanics of Earthquakes and Faulting.* Cambridge University Press.

[Toda and Stein, 2002] Toda, S. and Stein, R. S. (2002). Response of the San Andreas fault to the 1983 Coalinga Nuñez Earthquakes: An application of interaction-based probabilities for Parkfield. *J. Geophys. Res.*, 107.

[Utsu, 1965] Utsu, T. (1965). A method for determining the value of b in a formula $logn = a - bm$ showing the magnitude-frequency relation for earthquakes (with english summary). *Geophys. Bull. Hokkaido Univ.*, 13:99–103.

[Viso, 2004] Viso, Y. (2004). Stime dei parametri della legge di Gutenberg-Richter al contatto Alpi-Dinaridi. Thesis, Dip. di Scienze della Terra, University of Trieste.

[Wells and Coppersmith, 1994] Wells, D. L. and Coppersmith, K. J. (1994). New Empirical Relationships among Magnitude, Rupture Length, Rupture Width, Rupture Area and Surface Displacement. *Bull. Seism. Soc. Am.*, 84(4):974–1002.

[Živčić et al., 2000] Živčić, M., Suhadolc, P., and Vaccari, F. (2000). Seismic Zoning of Slovenia Based on Deterministic Hazard Computation. *Pure Appl. Geophys.*, 157:171–184.

Acknowledgments

Most of the study has been carried out while the author was working in the framework of the Project Interreg III A *Reti sismologiche senza confini nelle Alpi Orientali*.

The author wishes to thank Brian Kennett, for kindly providing the base code for the reflectivity method, and for the help in the debugging process of it, and Mladen Živčić and Jure Bajc for providing the picking data and for the cooperation in the JHD relocation.

Then, the author wishes to thank his tutor, Peter Suhadolc, for his patience and his calm guidance, all the staff of the *Dipartimento di Scienze della Terra - Università di Trieste*, in particular Giovanni Costa, and all the students, Phd students, post-docs and ex-colleagues for the cooperation and the time passed together.

Last but not least, the author wishes to thank all his friends and relatives, for the moral support and the encouragement.